

## Late Silurian–Early Devonian tuffites from the Małopolska and Łysogóry blocks reflect arc-back-arc magmatic activity on the southern margin of Laurussia

Emil WÓJCIK<sup>1,\*</sup>

<sup>1</sup> University of Warsaw, Faculty of Geology, Żwirki i Wigury 93, 02-089 Warszawa, Poland; ORCID: 0000-0002-5383-6018



Wójcik, E., 2023. Late Silurian–Early Devonian tuffites from the Małopolska and Łysogóry blocks reflect arc-back-arc magmatic activity on the southern margin of Laurussia. Geological Quarterly, 67: 47;  
<https://doi.org/10.7306/gq.1717>

Zircon U-Pb dating of tuffites within the upper Silurian greywackes in the southern part of the Holy Cross Fold Belt gives a result of  $419.91 \pm 1.7$  Ma, which indicates they are of Přídolí age. Geochemical studies of Přídolí tuffites from the Małopolska Block, an Emsian tuffite from the Łysogóry Block in the Holy Cross Fold Belt and a Přídolí tuffite from the Bardo Unit in the Central Sudetes indicate that they were formed in a similar tectonic setting related to post-orogenic, continental arc-back-arc magmatism, developed along the southern margin of Laurussia, correlated with the Rhenohercynian Zone. In terms of their geochemical pattern, the tuffites are similar to the upper Silurian–Lower Devonian igneous rocks in Germany, Ukraine (Podolia) and Moldova, which were probably formed along the same subduction zone, during an early stage of the continental arc-back-arc magmatic activity.

Key words: zircon ages, geochemistry, late Silurian magmatism, Holy Cross Mountains, Sudetes.

### INTRODUCTION

Manifestations of magmatic activity at the Silurian–Devonian boundary in Central Europe are very rare. In the geological literature, only a few examples of such magmatism from Poland have been described in detail: a diabase intrusion in the Bardo Syncline of the Holy Cross Fold Belt (Czarnocki, 1919; Kowalczewski and Lisik, 1974; Nawrocki et al., 2013; Fig. 1D and Table 1), the Kielce tuff (Malec, 2001; Krzemińska and Krzemiński, 2019; Fig. 1D and Table 1) and Niewachłów tuffites (Wójcik et al., 2021; Fig. 1D) from the northern part of the Małopolska Block; an upper Silurian granophyre diorite from the Sosnowiec IG 1 borehole (Table 1) in the Brunovistulian Block (Nawrocki et al., 2020) and a tuffite in the Ždanów section (Fig. 1B) in the Bardo Unit (BU) (Fig. 1A) in the Central Sudetes (Porębska, 1982; Wyżga, 1987). The tectonic setting of the Silurian–Devonian igneous event still raises questions: according to Nawrocki et al. (2020), the magmatic activity took place during extension of the back-arc basin in the Rhenohercynian Zone located on the southern margin of Avalonia. Krzemiński (2004) inferred that the diabase in the Bardo Syncline formed during detachment of the Małopolska Block from Baltica and the shift between them during Ludlow–Emsian time, while Krzemińska and Krzemiński (2019) considered that the Kielce tuff was formed during the prolonged collision of Baltica and Avalonia, in

the last phase of deformation in the basement of the Caledonian foreland.

This study analyses the tectonic setting of late Silurian–Early Devonian magmatic activity along the southern margin of Laurussia in the modern Central Europe, from the geochemical compositions of the Niewachłów tuffites (upper Silurian) of the Małopolska Block, the Barcza tuffite (Lower Devonian–Emsian) of the Łysogóry Block and the Ždanów tuffite (upper Silurian – Přídolí) of the Bardo Unit in the Central Sudetes. The ages of zircons from the Niewachłów tuffites (upper Silurian) were also determined. The results obtained were compared with published geochemical data for upper Silurian–Lower Devonian igneous and pyroclastic rocks in Germany (Rhenohercynian Zone, Mid-German Crystalline Zone), Ukraine (Podolia Region) and Moldova. The geochemical and spatial characteristics of these rocks enabled their location within Laurussia and demonstrate their relationship with the initial, extensional magmatism developed at the Silurian–Devonian transition, just before the opening of Rhenohercynian Ocean.

### GEOLOGICAL SETTING

The Precambrian crust of the East European Craton is separated from the Paleozoic Platform of central and western Europe by the Trans-European Suture Zone (TESZ) (Fig. 1A) (e.g., Berthelsen, 1992; Grad et al., 1999; Pharaoh et al., 2006). The TESZ is a significant tectonic zone measuring >2,000 km, stretching from the Black Sea in the south to the North Sea in the north. The structure of the TESZ, as well as the mechanism and time in which it formed, have not been clearly established

\*E-mail: emilwojciech@student.uw.edu.pl

Received: July 10, 2023; accepted: October 18, 2023; first published online: December 15, 2023

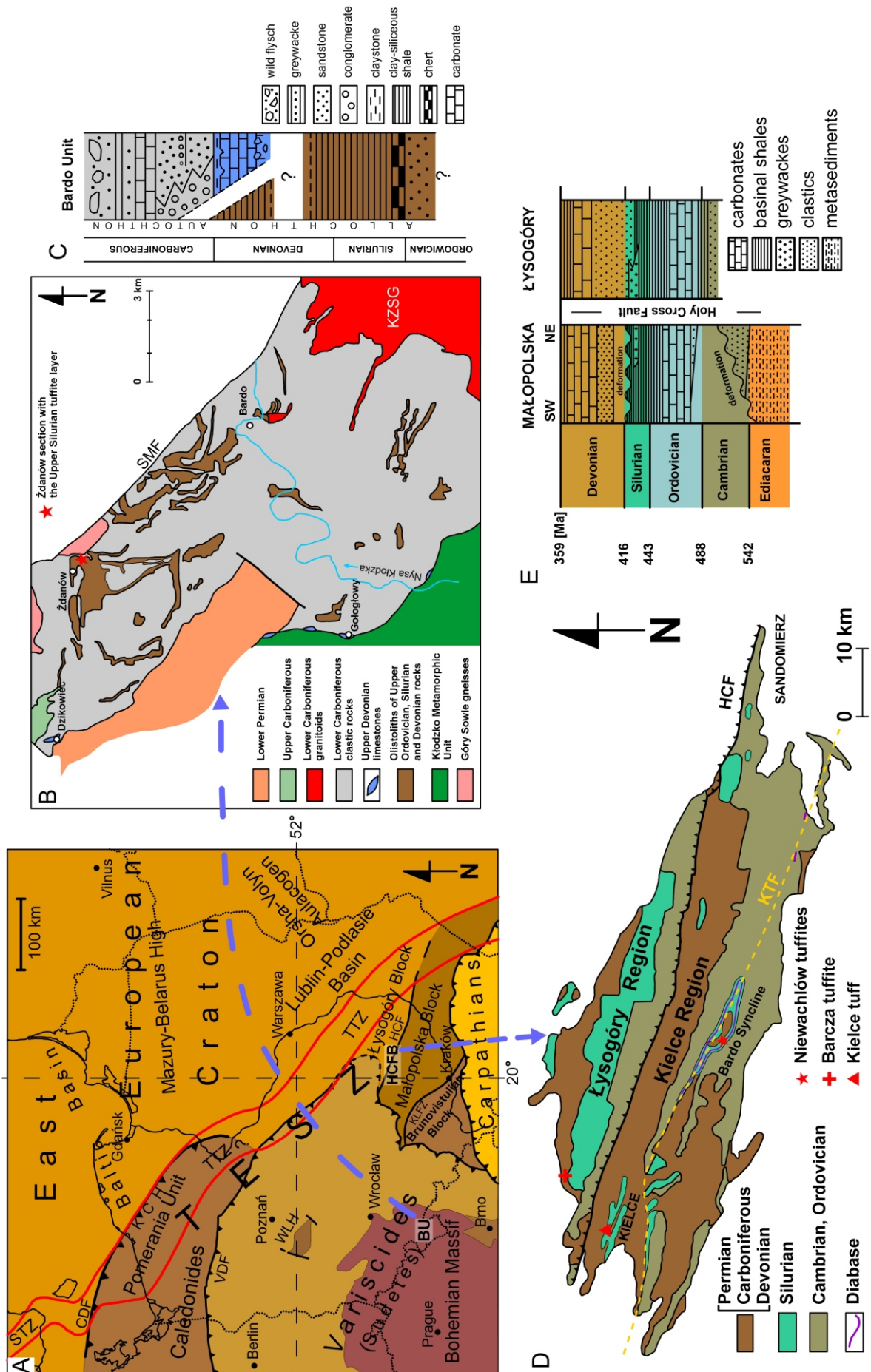


Fig. 1A – sketch tectonic map of Central Europe (after Nawrocki and Poprawa, 2006; modified); CDF – Caledonian Deformation Front; HCF – Holy Cross Fold Belt; BU – Bardo Unit; KCF – Kraków-Lubliniec Fault Zone; KLFZ – Krzysztof-Leszno High; VDF – Variscan Deformation Front; RI – Rügen Island; STZ – Sorgenfrei-Tornquist Zone; TESZ – Trans-European Suture Zone; TTZ – Teisseyre-Tornquist Zone; WHL – Wojsztyn-Leszno High; VDF – Variscan Deformation Front; B – geological map of the Bardo Mountains with location of the Ždanów section belonging to the Bardo Unit (after Kryza et al., 2011; Racki et al., 2022); C – simplified lithostratigraphic section of the Bardo Sedimentary Unit (after Mazur et al., 2006; Racki et al., 2022; modified); D – geological sketch map of the Holy Cross Fold Belt (after Nawrocki et al., 2007b; Malec et al., 2016; modified); KTF – Kielce–Tarnobrzeg Fault; E – generalized stratigraphy of the Lysogory and Małopolska Regions (after Walczak and Belka, 2017; modified)

Table 1

## Comparison of radiometric age data for Silurian and Lower Devonian magmatic rocks from the Brunovistulian and Małopolska blocks

Tectonic affiliation	Rock	Material	Method	Age [Ma]	Reference
Małopolska Block	Kielce tuff	zircon	U-Pb	414.2 ±6.6	Krzemińska and Krzemiński (2019)
	Niewachłów tuffites	zircon	U-Pb	419.91 ±1.7	this paper
	Bardo diabase	whole rock	Ar-Ar combined with geomagnetic polarity time scale	ca. 424–416	Nawrocki et al. (2013)
Brunovistulian Block	Velké Vrbno Dome amphibolite	zircon	U-Pb	407.5 ±2.5	Jastrzębski et al. (2021)
	Granophyre diorite from the Sosnowiec IG 1 borehole	zircon	U-Pb	420 ±2	Nawrocki et al. (2020)
	Hlina granite	garnet	Sm-Nd	430 ±6.4	Hönig (2016)
	Basaltic dike from Zelesice	whole rock	K-Ar	438 ±16	Přichystal (1999)

and are variously interpreted. Some researchers consider that the TESZ consists of many lithospheric blocks (like Pomerania, Łysogóry, Małopolska and Brunovistulian) belonging to the Paleozoic Platform, docked to the SW margin of the Baltica palaeocontinent during Cambrian to Carboniferous times (Pharaoh, 1999; Belka et al., 2002; Winchester et al., 2002a, 2006). Nawrocki and Poprawa (2006) and Pharaoh et al. (2006) suggested that the provenance of these blocks may be various, related to Baltica, Avalonia or other fragments of peri-Gondwana (Nawrocki and Poprawa, 2006; Grad et al., 2008; Narkiewicz et al., 2015; Narkiewicz and Petecki, 2017; Golonka et al., 2019; Źelaźniewicz et al., 2020). Others (Berthelsen, 1998; Smit et al., 2016; Mazur et al., 2015a, 2020, 2021) proposed that these blocks belonged to attenuated continental crust of the Baltica margin.

Although the origin of these blocks is much discussed, many researchers agree that before the Silurian, the Małopolska Block and the Łysogóry Block were connected with the margin of the Eastern European Craton (Nawrocki and Poprawa, 2006; Nawrocki et al., 2007a; Źelaźniewicz et al., 2009; Walczak and Belka, 2017; Mazur et al., 2020). Paleozoic rocks forming the Holy Cross Fold Belt (HCFB) are exposed at the surface on both sides of the border between the Małopolska and Łysogóry blocks (Fig. 1A; Czarnocki, 1919, 1957; Dadlez et al., 1994; Konon, 2008). The HCFB is traditionally divided into two parts: the Kielce Region (southern) and the Łysogóry Region (northern; Fig. 1D), differing in stratigraphy and structural evolution (Fig. 1E). The Kielce Region is separated from the Łysogóry Region by a WNW–ESE-oriented tectonic zone, named the Holy Cross Fault (Fig. 1D). This fault is also the border between the Małopolska and Łysogóry blocks including the Kielce and Łysogóry regions, respectively. The Holy Cross Fault was formed either in Devonian times as an oblique-slip fault under transtensional conditions (Lamarche et al., 2003) or around the Silurian–Devonian boundary as a thrust or reverse fault during late Caledonian deformation (Gagała, 2015).

An example of late Silurian magmatic activity in the Kielce Region is the diabase intrusion in the Bardo Syncline (Fig. 1D). The intrusion is located approximately at the boundary between lower Ludlow graptolite shales and middle Ludlow greywackes (Czarnocki, 1939; Kowalczewski and Lisik, 1974). Ar-Ar isotopic dating of this diabase by Nawrocki et al. (2013) indicated an age of ~416–424 Ma (Table 1) which is close to the Silurian–Devonian boundary. This rock has a composition of tholeiitic basalt, which formed in an extensional tectonics regime (Krzemiński, 2004), being intruded into the Silurian strata be-

fore folding (Kowalczewski and Lisik, 1974). According to Nawrocki et al. (2007b), the diabase magma utilised the WNW–ESE-oriented Kielce–Tarnobrzeg Fault that extends over the entire Kielce Region (Fig. 1D). The graptolite shales belong to the Pragowiec Beds (late Wenlock–early Ludlow) (Tomczykowa and Tomczyk, 1981; Malec, 2006) and contain 9 K-bentonite beds described by Langier-Kuźniarowa and Ryka (1972). Above the diabase in the Bardo Syncline (Fig. 1D), the upper Silurian greywackes of the Niewachłów Beds (middle Ludlow–lower Ludfordian; Tomczyk, 1962; Tomczykowa and Tomczyk, 1981; Stupnicka, 1995; Malec, 2001, 2006; Kozłowski et al., 2014) contain interbeds, the Niewachłów tuffites (Fig. 2; Wójcik et al., 2021). The petrographic composition of the Niewachłów tuffites indicate (Wójcik et al., 2021) that they originated from high-potassic dacitic magma. These tuffites were deformed in the early Carboniferous and early Permian due to activation of the Daleszyce Fault Zone (Wójcik et al., 2021). Another layer of tuff produced by late Silurian magmatism occurs in the Kielce Beds in the city of Kielce (Malec, 2001; Fig. 1D). The age of the Kielce tuff was determined by U-Pb dating of zircons at 414.2 ±6.6 Ma (Krzemińska and Krzemiński, 2019; Table 1).

In the Kielce Region (part of the Małopolska Block) a stratigraphic gap extends above the greywacke rocks of the upper Ludlow, related to late Caledonian deformation of the HCFB (Fig. 1E), which did not take place in the Łysogóry Region (Czarnocki, 1936; Malec, 2001; Kozłowski et al., 2014; Malec et al., 2016). Lower Devonian (Emsian) siliciclastic rocks were deposited with an angular unconformity on the Niewachłów graywacke (Fig. 1E) in the Kielce Region (Czarnocki, 1919; Racki, 2006). The same Lower Devonian deposits are also present in the Łysogóry Region (Fig. 1E), but without angular unconformity. These rocks contain many layers of tuffite and bentonite (Tarnowska, 1971, 1976). The thickest tuffite unit (up to 1.5 m) occurs in Emsian sandstone on the Barcza Mountain (Figs. 1D and 2) in the Łysogóry Region (Kardymowicz, 1960a; Fijałkowska-Mader and Malec, 2018).

The other area of Poland where products of late Silurian volcanism are observed is the Bardo Unit (Fig. 1A, B) in the Central Sudetes, which includes Ordovician, Silurian, Devonian and Carboniferous deposits (Fig. 1C; Wyżga, 1987; Franke et al., 1993; Racki et al., 2022). The similarity of the terms Bardo Unit (Central Sudetes; Fig. 1A, B) and Bardo Syncline (Holy Cross Fold Belt; Fig. 1A, D) is only coincidental.

Ordovician to Lower Devonian rocks of the Bardo Unit (Central Sudetes) occur in allochthonous position (Fig. 1C),

preserved as olistoliths in the Carboniferous synorogenic succession (Wajsprych, 1978; Chorowska, 1990) belonging to a Variscan accretionary prism (Franke et al., 1993; Mazur et al., 2015b; Racki et al., 2022). The Bardo Unit lies partly on the Central Sudetes Ophiolites, the Sowie Góry Massif and the Kłodzko Metamorphic Unit (Mazur et al., 2006). Sedimentation of the Ordovician, Silurian and Lower Devonian rocks of the Bardo Unit may originally have taken place in the southern part of the Rheic Ocean (Porębska and Sawłowicz, 1997). According to Chorowska (1990), upper Silurian and Lower Devonian claystones and mudstones contain numerous tuffite layers and volcanic breccia of rhyolitic type. One of the best examples of volcanic activity preserved in the lower Paleozoic strata of the Bardo Unit is the tectonically deformed tuffite layer ~50 cm thick (Fig. 2), located in upper Silurian (Přídolí) graptolite shales, just beneath the stratigraphic boundary with Lower Devonian rocks (Fig. 2; Porębska, 1982; Wyżga, 1987).

## SAMPLES AND METHODS

The following samples were selected for the geochemical bulk-rock analysis: one sample of tuffite from the Ždanów section (Figs. 1B, 2 and 3F) ( $50^{\circ}33'44.5''N$   $16^{\circ}39'56.1''E$  Google Maps) in the Central Sudetes; three samples of Niewachłów tuffites from Czyżów (T0, T1, T2; Figs. 1D, 2 and 3A) ( $50^{\circ}44'28.5''N$   $21^{\circ}00'06.9''E$  Google Maps) and one sample of tuffite from Barcza Mountain (Western Quarry; Figs. 1B, 2 and 3E;  $50^{\circ}57'25.1''N$   $20^{\circ}43'30.5''E$  Google Maps) in the Holy Cross Fold Belt. The samples were pulverized in an agate mill before sending to the laboratory. Whole-rock analyses were performed at the ACME Bureau Veritas Analytical Laboratory in Vancouver, Canada. Major elements were analysed by Inductively Coupled Plasma Emission Spectrometer (ICP-OES), and trace elements, including REE, by Inductively Coupled Plasma Mass Spectrometry (ICP-MS). Detection limits are within 0.01% for major elements, between 0.1–0.5 ppm for most trace elements, 1 ppm for Ba, Sn and Zn, and 8 ppm for V. Geochemical diagrams were made using *GCDKit* software (Janoušek et al., 2006).

Zircon crystals were isolated from the T1 layer (Fig. 3A) of the Niewachłów tuffites (Fig. 2) for the isotopic age analysis. In order to remove clay minerals, each tuffite sample was rinsed 60 times in water. The magnetic fraction (including biotite; Fig. 3C) was separated with a neodymium magnet. The same magnetic fraction was gently pulverized in an agate mortar and secondly subjected to the action of a neodymium magnet to separate the non-magnetic minerals that occur as inclusions, mainly in biotite grains (Fig. 3B). These non-magnetic minerals include many zircon crystals which can be separated with a microdissection needle and a binocular microscope without using heavy liquids (Fig. 3D). Then, the zircons were mounted in epoxy resin and polished. Cathodoluminescence images of zircons were carried out on carbon-coated samples using a Cameca SX-100 Electron Microprobe (15 kV) at the Faculty of Geology, University of Warsaw, Poland.

*In situ* U-Pb zircon dating by laser ablation inductively coupled plasma mass spectrometry (LA-ICP-MS) was performed at the Kraków Research Centre, Institute of Geological Sciences, Polish Academy of Sciences. The analyses were conducted using an excimer laser (ArF) *RESOlution* M-50 by Resonetics (now Applied Spectra) coupled with an ICP-MS XseriesII by Thermo Fisher Scientific. Detailed description of the LA-ICP-MS and the analytical conditions applied have been described by Anczkiewicz and Anczkiewicz (2016). Concordia

U-Pb zircon ages, mean ages and diagrams were generated using *Isoplot R* software (Vermeesch, 2018).

## RESULTS

### IN SITU U-PB (LA-ICP-MS) ZIRCON DATING

U-Pb dating was applied to the zircon crystals from the T1 layer of the Niewachłów tuffites (Appendix 1). Almost all the zircons separated are pale yellow, elongated, euhedral crystals (Fig. 3D) indicating their volcanic origin. Only a few crystals are partially rounded (Fig. 3D), but they are also pale yellow. Cathodoluminescent images revealed zircon growth zones oriented along the elongated direction of the crystals (Fig. 4B). Most of the zircons contain an inherited core; only a few display homogeneous structure. Only analysis of homogeneous zircons and external crystal growth zones were selected to calculate the concordia age (Appendix 1). The calculation was performed on 14 analyses (the youngest analysis was excluded from calculation due to the uncertainty and extreme measurement). The concordia age calculated is  $419.91 \pm 1.7$  Ma (MSWD = 0.45; Fig. 4A), mean age  $420.03 \pm 1.75$  Ma (MSWD = 0.77; Fig. 4C), constraining the deposition time of the T1 layer of the Niewachłów tuffites to the late Silurian (Přídolí). The frequency distribution of all analyses (33 points; Fig. 4D) shows that apart from the last volcanic episode corresponding to the formation of tuffite in the Přídolí, there are also results indicating an age of ~433 Ma (Wenlock) related to inherited zircon cores.

### GEOCHEMISTRY OF THE PYROCLASTIC ROCKS AND TECTONIC IMPLICATIONS

The main components of the Niewachłów tuffites (Upper Silurian – HCFB) are  $\text{SiO}_2$  (56.30–61.71 wt.%),  $\text{Al}_2\text{O}_3$  (16.35–20.80 wt.%),  $\text{MgO}$  (1.52–1.90 wt.%),  $\text{Na}_2\text{O}$  (0.23–0.60 wt.%),  $\text{Fe}_2\text{O}_3$  (3.97–5.33 wt.%),  $\text{TiO}_2$  (0.78–0.95 wt.%),  $\text{CaO}$  (0.38–0.93 wt.%),  $\text{K}_2\text{O}$  (4.36–5.94 wt.%),  $\text{MnO}$  (0.03 wt.%),  $\text{P}_2\text{O}_5$  (0.11–0.49 wt.%) and  $\text{Cr}_2\text{O}_3$  (<0.01–0.016 wt.%; Table 2). The Barcza tuffite (Lower Devonian – HCFB) differs in the lower content of  $\text{CaO}$  (0.15 wt.%),  $\text{Na}_2\text{O}$  (<0.01 wt.%),  $\text{MnO}$  (<0.01 wt.%),  $\text{TiO}_2$  (0.21 wt.%),  $\text{P}_2\text{O}_5$  (0.04 wt.%) and a higher concentration of  $\text{MgO}$  (4.37 wt.%) and  $\text{K}_2\text{O}$  (7.36 wt.%; Table 2). The tuffite from Ždanów (upper Silurian – Central Sudetes), compared to the Niewachłów tuffites, has a lower share of  $\text{MgO}$  (1.36 wt.%), significantly lower  $\text{K}_2\text{O}$  (0.75 wt.%) but more  $\text{Fe}_2\text{O}_3$  (7.21 wt.%),  $\text{Na}_2\text{O}$  (2.7 wt.%),  $\text{MnO}$  (0.76 wt.%) and  $\text{Cr}_2\text{O}_3$  (0.07 wt.%; Table 2).

All samples investigated are pyroclastic rocks that underwent tectonic deformation or hydrothermal alteration (Kardymowicz, 1960b; Wyżga, 1987; Wójcik et al., 2021). Hydrothermal activity does not appear to have affected the REE content (Fig. 5G) of these samples because they do not show a positive Eu anomaly (Barret et al., 1990; Douville et al., 1999). Nevertheless, these processes could have changed the chemical composition of the rocks, especially in relation to mobile elements. Therefore, the basic characteristics of the source magma were determined using a Co vs. Th diagram (after Hastie et al., 2007) which was constructed for altered rocks. In the Co vs. Th diagram (Fig. 5A), all samples are located in the field of igneous rocks of the high potassic calc-alkaline and shoshonite series. The classification diagram of volcanic rocks Nb/Y vs.  $\text{Zr}/\text{TiO}_2$  (Fig. 5B) shows that three samples of Niewachłów tuffite (Fig. 3A; upper Silurian – HCFB) correspond

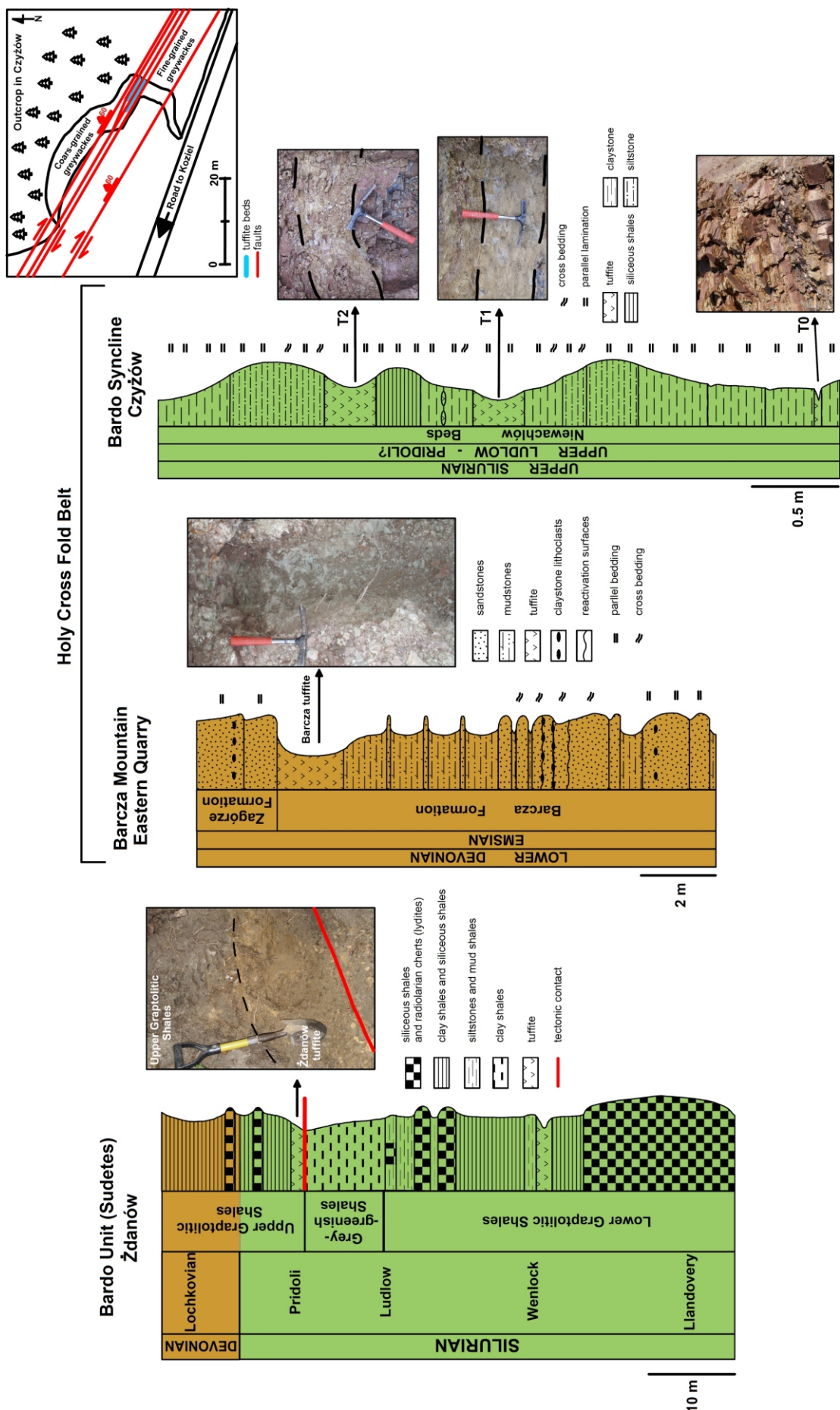
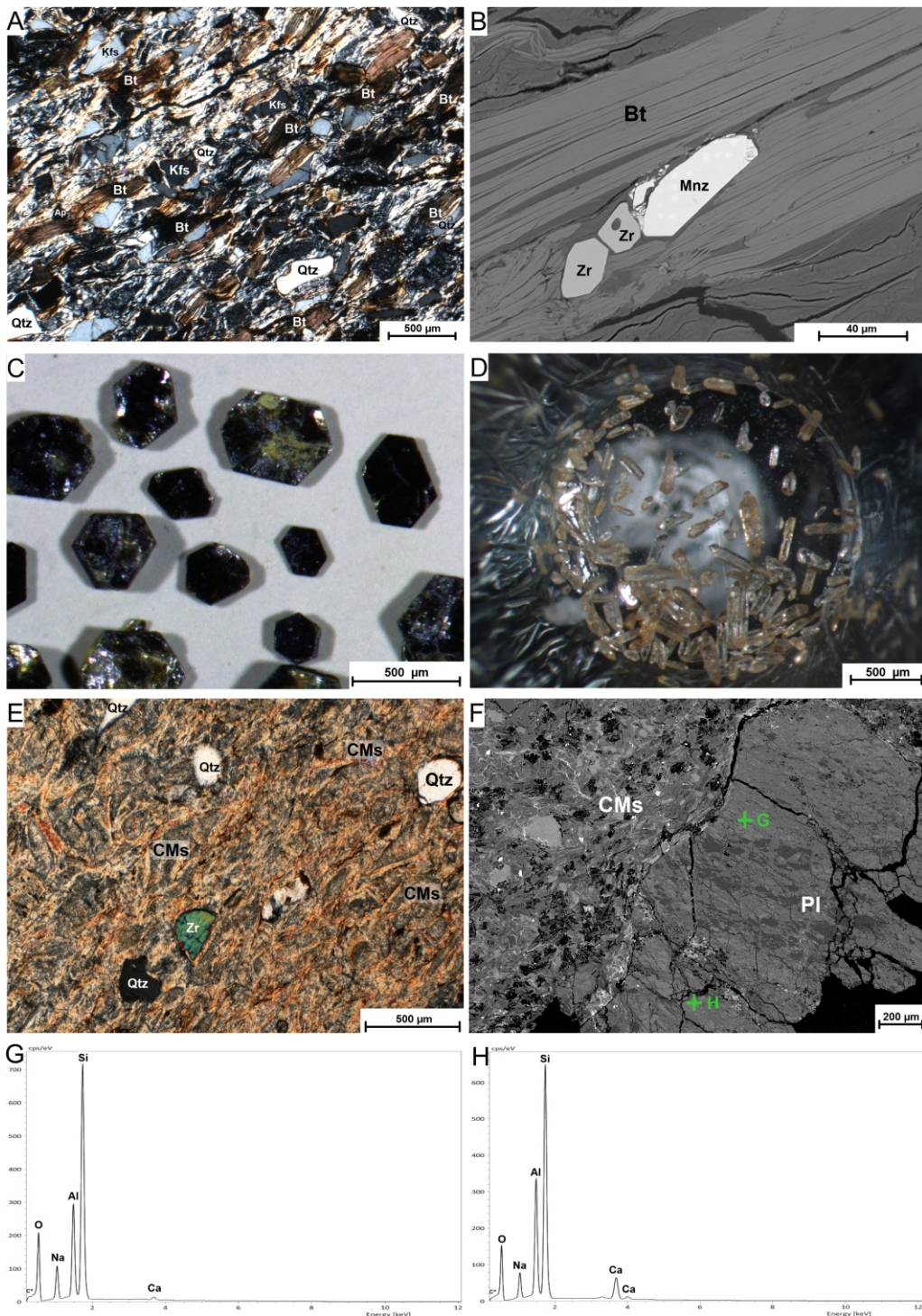
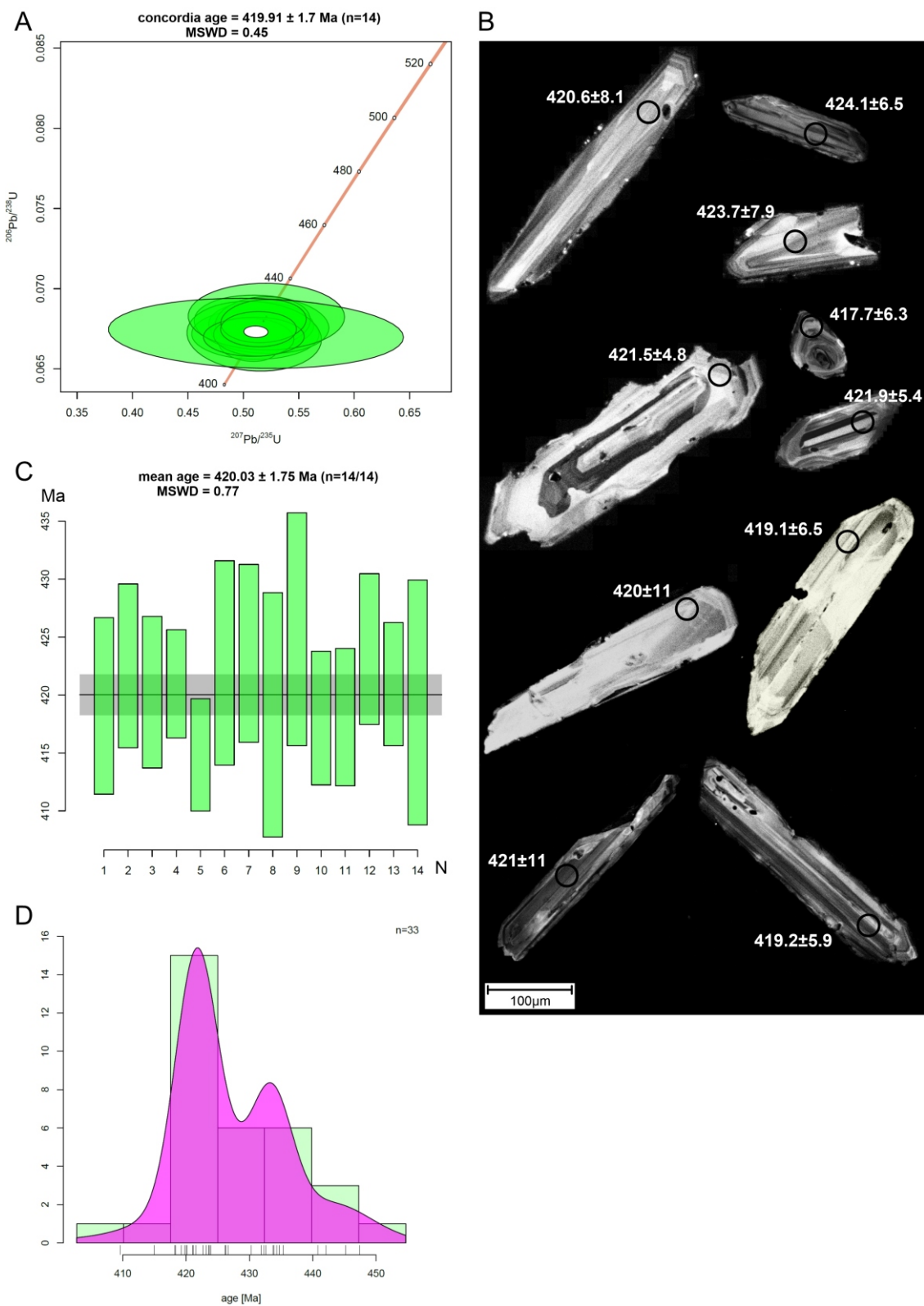


Fig. 2. Lithostratigraphic columns with parts of sections investigated containing tuffite beds

Part of the Źdanów section with the Źdanów tuffite (after Kremer, 2006, modified); Eastern Quarry section (Barcza Mountain) with the Barcza tuffite (after Fijałkowska–Mader and Malec, 2018, modified); part of the Czyżów section with Niewachłów tuffite layers (T0, T1, T2) and a schematic map of the outcrop in Czyżów (after Wójcik et al., 2021, modified)



**Fig. 3A –** thin-section microphotograph showing the proportion of the main mineral components (biotite, quartz and K-feldspar) in the T1 layer of the Niewachłów tuffites, crossed polars; **B –** SEM image of zircon-monazite inclusions in biotite (T2 layer of the Niewachłów tuffites); **C –** binocular microscope image of relatively thick euhedral biotite crystals from the Niewachłów tuffites (T1 layer); **D –** binocular microscope image of pale yellow zircons separated from the Niewachłów tuffites (T1 layer) at the bottom of the test tube; **E –** thin-section microphotograph showing the mineral composition of the Barcza tuffite, the clay minerals probably formed as a result of volcanic glass and feldspar alteration, crossed polars; **F –** backscatter SEM image showing the Ždanów tuffite with altered plagioclase; **G, H –** SEM EDS analysis of altered plagioclase from photo "F" (Ždanów tuffite), Bt – biotite, Kfs – k-feldspar, Qtz – quartz, PI – plagioclase, Ap – apatite, Zr – zircon, Mnz – monazite, CMs – clay minerals



**Fig. 4. Results of U-Pb (LA-ICP-MS) zircon dating analyses from the T1 layer of the Niewachłów tuffites**

**A** – concordia U-Pb diagram; **B** – cathodoluminescence microphotographs with LA-ICP-MS ages of representative zircons; **C** – zircon U-Pb weighted mean age; **D** – histogram showing results of zircon dating analysis

Table 2

**Major and trace element geochemistry of upper Silurian and Lower Devonian samples from Poland**

Sample	Niewachłów tuffites			Barcza tuffite	Żdanów tuffite
	T0	T1	T2		
Geographical coordinates	50°44'28.5"N 21°00'06.9"E			50°57'25.1"N 20°43'30.5"E	50°33'44.5"N 16°39'56.1"E
Location	Outcrop in Czyżów			Barcza Mountain (Western Quarry)	Żdanów section
Major oxides (wt.%)					
SiO <sub>2</sub>	61.71	56.3	61.1	60.64	60.36
Al <sub>2</sub> O <sub>3</sub>	16.35	22.8	20.8	16.42	16.17
Fe <sub>2</sub> O <sub>3</sub>	5.33	4.15	3.97	4.05	7.21
CaO	0.38	0.93	0.59	0.15	0.67
MgO	1.52	1.9	1.52	4.37	1.36
Na <sub>2</sub> O	0.6	0.3	0.23	<0.01	2.7
K <sub>2</sub> O	4.36	5.94	5.02	7.36	0.75
MnO	0.03	0.03	0.03	<0.01	0.76
TiO <sub>2</sub>	0.84	0.95	0.78	0.21	0.79
P <sub>2</sub> O <sub>5</sub>	0.11	0.49	0.28	0.04	0.2
Cr <sub>2</sub> O <sub>3</sub>	0.016	<0.01	<0.01	<0.01	0.07
SO <sub>3</sub>		0.145	0.012		
Trace elements (ppm)					
Ba	742	3068	771	12	274
Be	3	1	<1	6	<1
Co	4.9	10.5	10.9	11.7	17.3
Cs	14.1	4.9	5.3	9.1	1
Ga	15.9	22.9	19.1	23.5	15.9
Hf	11.8	15.4	11.5	10.5	4.2
Nb	14.9	39.3	31.8	26.5	6.5
Rb	122.6	105	99.6	108.3	28.8
Sn	2	5	4	5	<1
Sr	50.8	36.8	25.6	6.2	86.2
Ta	1.1	2.3	2.2	2.1	0.5
Th	12.4	29	22.3	23.3	11.9
U	3.9	6.3	5.1	5.9	2.5
V	102	50	60	8	176
W	1.5	2.7	2.1	1.7	1
Zr	449.8	558.6	421.9	294.6	150.2
Y	32.4	105.4	76	48	22.7
La	34.3	85.1	57.1	12.9	21.2
Ce	62.1	189.9	136.7	35.8	43.5
Pr	8.25	24.29	18.22	4.46	5.26
Nd	31.8	97.7	74.5	18.5	20.8
Sm	6.17	21.8	17.44	4.89	4.26
Eu	1.22	2.29	2.38	0.78	1.17
Gd	5.79	21.66	17.35	5.76	4.85
Tb	0.87	3.4	2.53	1.22	0.72
Dy	5.39	19.3	14.64	8.59	4.15
Ho	1.11	3.96	2.87	1.89	0.81
Er	3.29	11.67	8.2	5.9	2.28
Tm	0.49	1.63	1.13	0.86	0.3
Yb	3.2	10.37	7.13	5.78	1.93
Lu	0.51	1.53	1.04	0.87	0.29
Mo	2.9	1.4	1.3	<0.1	0.3
Cu	37.8	7.1	38	2.5	37.3
Pb	67.2	9.6	10.2	0.7	6
Zn	303	61	39	22	61
Ni	22.2	12.6	17.7	16.8	266
As	38.2	1.4	4.5	2.5	0.5
Cd	0.6	0.1	<0.1	<0.1	0.1
Sb	0.3	<0.1	0.1	<0.1	<0.1
Bi	0.2	0.3	0.3	0.2	0.1
Ag	0.3	<0.1	<0.1	1	0.6
Au	2.2	1.1	0.9	<0.5	0.5
Hg	0.03	<0.01	0.02	<0.01	0.03
Tl	1	0.4	0.5	0.01	<0.1
Se	<0.5	<0.5	0.9	<0.5	3.1
Eu/Eu*	0.63	0.32	0.42	0.45	0.79

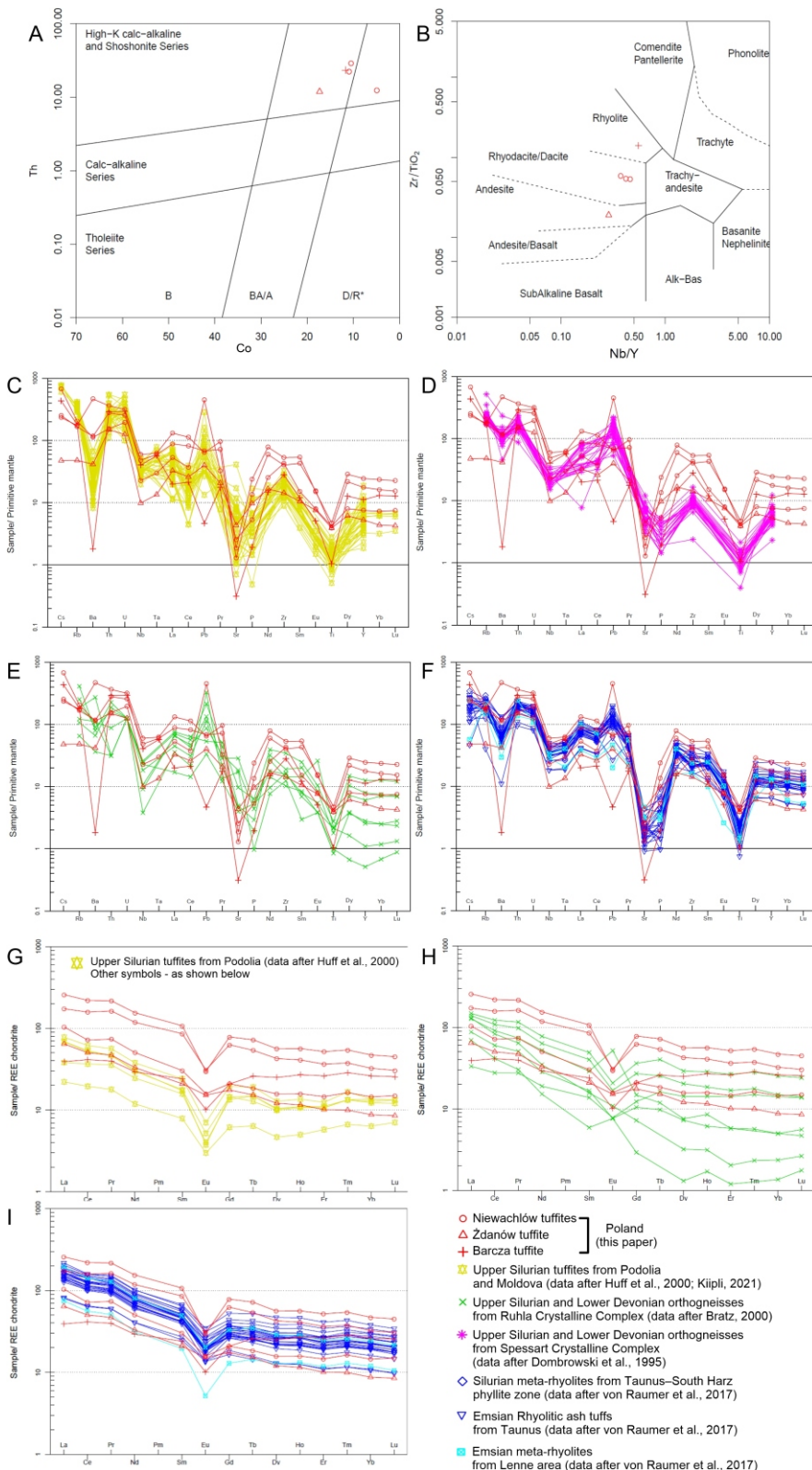


**Fig. 5A – Th vs. Co discrimination diagram for classifying altered volcanic rocks (after Hastie et al., 2007); B – classification of the volcaniclastic rocks studied on a Zr/TiO<sub>2</sub> vs. Nb/Y chemical discrimination diagram (after Winchester and Floyd, 1977); C, D, E, F – primitive mantle-normalized trace element spider diagrams (after McDonough and Sun, 1995) for the upper Silurian–Lower Devonian tuffites and volcanic or metavolcanic groups; G, H, I – REE patterns normalised to chondrite values (after Nakamura, 1974), for the upper Silurian–Lower Devonian volcanic or metavolcanic groups**

to rhyodacitic/dacitic composition, consistent with the petrographic classification of these rocks by Wójcik et al. (2021). The tuffite from Barcza (Fig. 3E; Lower Devonian – HCFB) has a rhyolitic composition (Fig. 5B), while the tuffite from Ždanów (Fig. 3F; upper Silurian – Central Sudetes) correspond to andesitic composition (Fig. 5B). The chondrite-normalized rare earth elements (REE) spider diagram (after Nakamura, 1974) shows a very high content of these elements in the samples studied from Poland (Fig. 5G), which however, differ from each other even within one section. The Niewachłów tuffites and the tuffite from Ždanów are characterized by enrichment in light rare earth elements (LREE: La–Pm) in relation to heavy rare earth elements (HREE: Ho–Lu; Fig. 5G; REE division after Grawunder et al., 2014; Migaszewski et al., 2016), while the tuffite from Barcza Mountain lacks this trend. Samples T1 and T2 (Fig. 2) from the Niewachłów tuffites show a very strong Eu anomaly (Fig. 5G), and sample T0, from 1 m below in the excavation (Fig. 2), has a distinctly lesser negative Eu anomaly (Fig. 5G). A strong Eu anomaly is also present in the tuffite from Barcza Mountain (HCFB), but the tuffite from Ždanów in the Central Sudetes barely has this anomaly (Fig. 5G). A strong negative europium anomaly in some of these samples (Fig. 5G) is accompanied by a lacking or negative Pb anomaly (Fig. 5C), which indicates fractional crystallization of magma. Sample T0 from the Niewachłów tuffites and the Ždanów tuffite sample show (Fig. 5G) a shallow or disappearing Eu anomaly with a positive Pb anomaly (Fig. 5C). The characteristics of these Eu anomalies are probably the result of the presence of plagioclase phenocrysts (Fig. 3F–H) in the melt. Whereas, the positive Pb anomalies (Fig. 5C) can be related to partial melting during arc magmatism or post-depositional Pb contamination of the samples by hydrothermal fluid migration (Hofmann, 1997).

Primitive-mantle normalized trace element compositions (Fig. 5C) of all the samples from Poland reveal negative anomalies of Nb, Ta, Ti, Sr, P; additionally, in the tuffites from Barcza Mountain and Ždanów there is a negative Ba anomaly (Fig. 5C). Nb, Ta, Ti anomalies (Fig. 5C) are considered as subduction zone indicators (Arculus and Powell, 1986; Elliott, 2003), which corresponds to the Th–Zr/117–Nb/16 discrimination diagram (after Wood, 1980; Fig. 6B), where all points plot as one group in the Continental Arc Basalt (CAB) field. These anomalies are shallow (especially in relation to the Niewachłów tuffites and the Barcza tuffite) (Fig. 5C), which, together with the high-potassic character of the samples (Fig. 5A), may indicate their post-collisional setting. The high content of Nb (14.9–39.3 ppm) and Ta (1.1–2.3 ppm; Table 2) in the samples from the Holy Cross Fold Belt according to Li et al. (2021) significantly exceeds the threshold value for arc magmatism [Nb (12.20 ppm) and Ta (0.796 ppm)] and may be compared with the back-arc magmatism of the Japan Sea or Patagonia. This observation is supported by the Rb vs. Y+Nb tectonomagmatic discrimination diagrams for granitoids (Fig. 7), according to which the tuffite samples from Poland plot in a post-collisional setting in the fields of Within Plate Granite (WPG) and Volcanic Arc Granite (VAG). Similarly, the Nb vs. Y diagram (Fig. 7) ranks all HCFB samples in the domain of Within Plate Granite (WPG). The exception is the tuffite from Ždanów in the Central Sudetes, corresponding to Volcanic Arc Granite and syn-Collisional Granite (Fig. 7). The Ždanów tuffite also contains less Nb (6.5 ppm) and Ta (0.5 ppm; Table 2), which indicates its greater relationship with a subduction zone; therefore, it was probably the result of continental arc magmatism.

Summing up, the geochemical patterns of the rocks studied indicate that they are related to the subduction zone (Fig. 5C) that stretched along the continental margin (Fig. 6B) but only the Ždanów tuffite has a clear arc magmatic signature (Fig. 7).

The rest of the samples from Poland (Niewachłów tuffite and Barcza tuffite) show a high-potassic character (Fig. 5A), post-collisional signatures (Fig. 7) and small negative Nb and Ta (Fig. 5C) anomalies, indicating extensional tectonic conditions. Therefore the high content of Nb (14.9–39.3 ppm) and Ta (1.1–2.3 ppm) in the samples imply magmatic activity during crustal thinning in a back-arc system (comp. Liu et al., 2018; Li et al., 2021), which developed simultaneously with an active arc (Ždanów tuffite) in front.

## INTERPRETATION AND DISCUSSION

### INTERPRETATION OF U–PB DATING RESULTS

The age of the Niewachłów Beds, in which the Niewachłów tuffites occur, were previously determined palaeontologically as middle Ludlow (Tomczyk, 1962; Tomczykowa and Tomczyk, 1981; Stupnicka, 1995; Malec, 2001, 2006; Kozłowski et al., 2014). In addition, Kozłowski and Tomczykowa (1999) included these rocks within the *Bohemograptus bohemicus* Zone on the basis of the trilobite and graptolite assemblages. Nevertheless the time range of the upper Silurian strata in the Kielce Region is still unclear and has been repeatedly reinterpreted over last few decades (Stupnicka et al., 1991, 1995; Malec, 1991, Malec, 1993, 2000, 2001, 2006, 2014; Modliński and Szymański, 2001 and references cited therein), due to the lack of continuous exposure and of index fossils. Thus, it cannot be ruled out that rocks younger than the middle Ludlow occur in the Bardo Syncline. New zircon U–Pb dating of the Niewachłów tuffites yielded an age of  $419.91 \pm 1.7$  Ma (Přídolí; Fig. 4A) for the T1 layer (Fig. 2), which is significantly younger than the age of the Niewachłów Beds determined palaeontologically. The exposure with tuffites is cut by several faults (Fig. 2) belonging to the Daleszyce Fault Zone responsible for the tectonic excision of two-thirds of the Silurian succession in the southern limb of the Bardo Syncline (Wójcik et al., 2021). These faults probably separate part of the upper Silurian section with tuffites from the Niewachłów Beds included in the middle Ludlow by Tomczyk (1962), Tomczykowa and Tomczyk (1981), Kozłowski and Tomczykowa (1999) and Kozłowski et al. (2014). The Niewachłów tuffites occur within unfossiliferous greywackes (siltstone, claystone and siliceous shale partly weathering to a red clay; Fig. 2). In the eastern and central parts of the Kielce Region, the Niewachłów Beds are overlain by the Lipniczek Beds (siltstone, claystone with thinly layered fine-grained greywacke sandstones) of variously interpreted age, as upper Ludlow or Přídolí (Tomczyk, 1962; Modliński and Szymański, 2001, Malec, 2006). The lithological characteristics of the rocks containing the Niewachłów tuffites are similar to those of the Lipniczek Beds, which corresponds to the Přídolí from U–Pb dating. This indicates that the rocks investigated probably belong to a younger section of the Niewachłów Beds than the middle Ludlow greywackes in the Bardo Syncline, being separated by the Daleszyce Fault Zone. Therefore the U–Pb dating shows that part of the Niewachłów Beds section with tuffites may also include Přídolí strata (Fig. 2).

### TUFFITES FROM POLAND WITH RESPECT TO THE MAGMATISM ALONG THE SOUTHERN MARGIN OF LAURUSSIA

Magmatic activity along the NE margin of Avalonia during the collision with Baltica and the closure of the Tornquist Ocean at the Ordovician–Silurian transition (Torsvik and Rehnström, 2003) produced many Silurian bentonite layers in the Baltic Basin (Batchelor and Jeppsson, 1999; Obst et al., 2002;

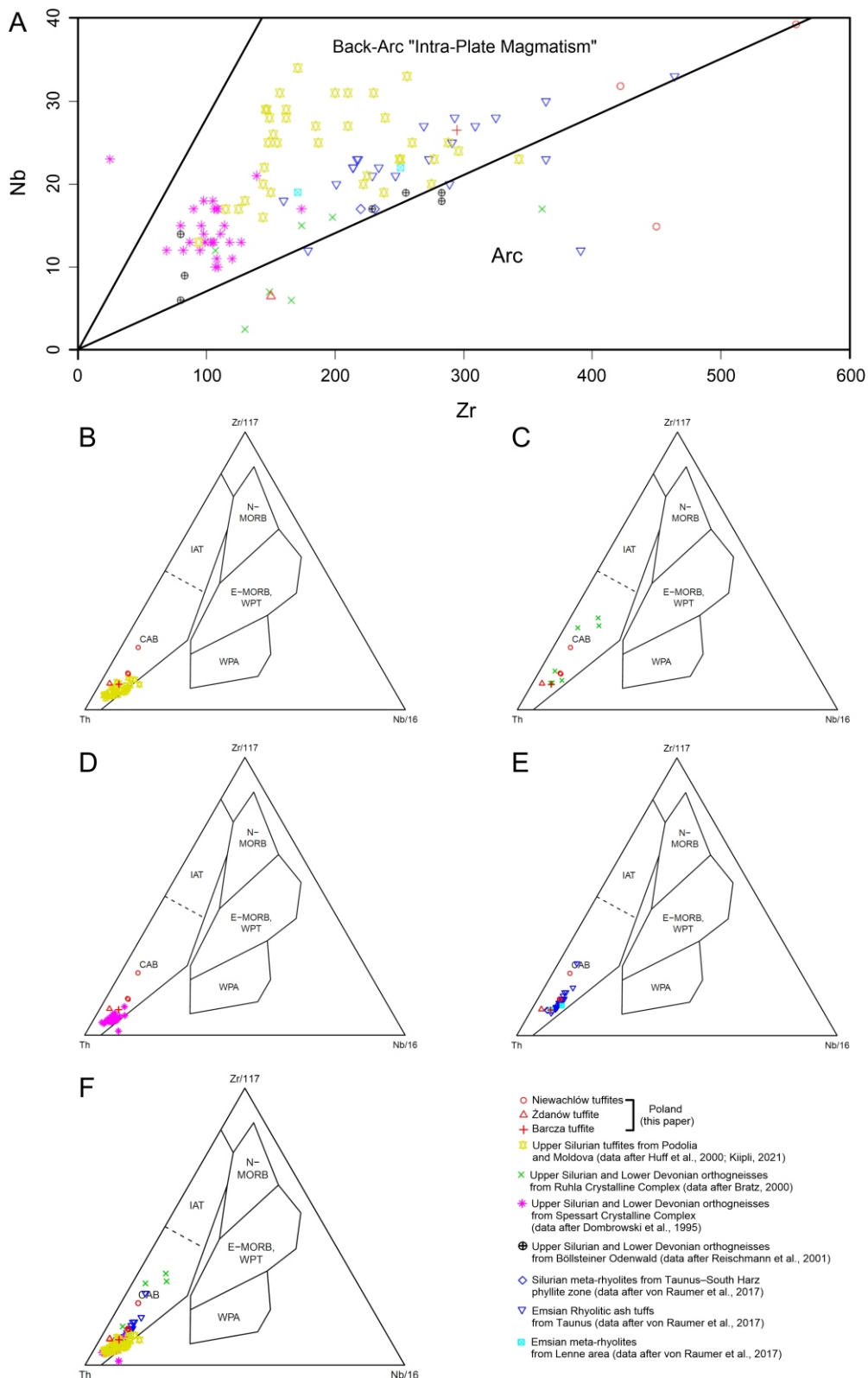


**Fig. 6A – Nb/Zr ratios for rocks from the southern margin of Laurussia compared with the compositional field of back-arc “Intra-Plate Magmatism” in New Zealand and Patagonia (after Tatsumi et al., 1995); B, C, D, E, F – Zr/117–Th–Nb/16 tectonic discrimination diagrams (after Wood, 1980) for samples from the southern margin of Laurussia (except for Böllsteiner Odenwald, with no data)**

CAB – Continental Arc Basalts, IAT – Island Arc Tholeiite, WPA – Within Plate Alkaline, WPT – Within Plate Tholeiite, E-MORB – Enriched Mid-Ocean Ridge Basalts, N-MORB – Normal Mid-Ocean Ridge Basalts

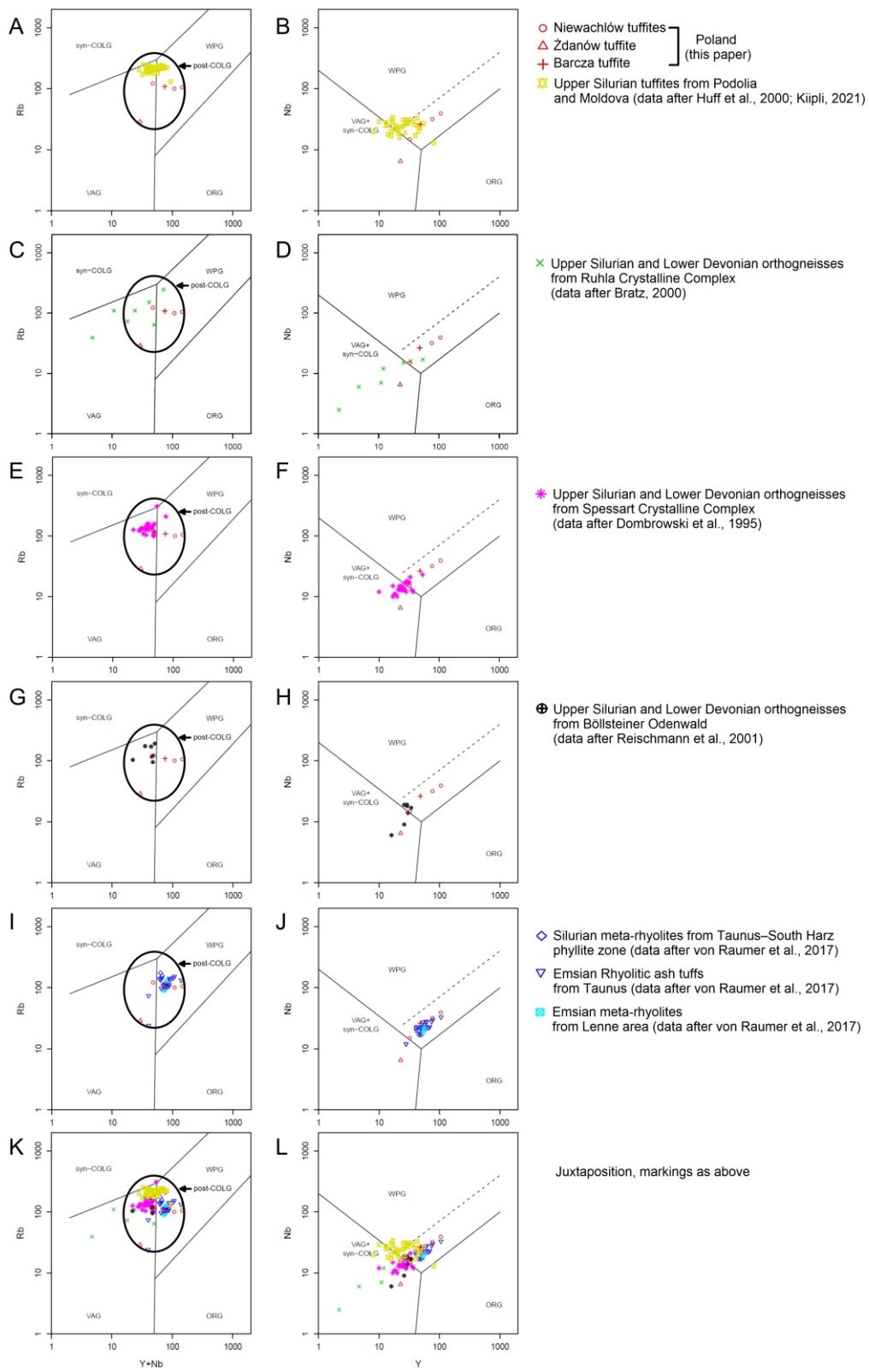


**Fig. 7. Rb vs. Y+Nb and Nb vs. Y tectonomagnetic diagrams for granitoids (after Pearce et al., 1984) with modification of post-collisional field from Pearce (1996) – left column**

syn-COLG – syn-Collisional Granite, WPG – Within Plate Granite, ORG – Oceanic Ridge Granite, VAG – Volcanic Arc Granite, post-COLG – Post-Collisional Granite

Anczkiewicz et al., 2017). Nevertheless, Ludlow bentonites from the southern part of the Baltic Basin differ from the tuffites investigated in this paper. According to Anczkiewicz et al. (2017) those bentonites are poorly enriched in incompatible light REEs with a very shallow or absent Eu anomaly, without affinity to a subduction zone. Additionally, the termination of collision caused an almost complete absence of pyroclastic deposits younger than the middle Ludlow across most of the Baltic Basin area (Fortey et al., 1996; Kipli et al., 2013, 2014). The Niewachłów tuffites are dated as Přídolí in age (Fig. 4), similarly to the tuffite from Ždanów (Porebska, 1982; Fig. 2), while the tuffite from Barcza Mountain is Emsian in age (Fig. 2) (Fijałkowska-Mader and Malec, 2018). Therefore, they were formed after the termination of the Caledonian magmatic activity in the Baltica/Avalonia collision zone and should have originated from a different source.

Another possible source area for the tuffites from Poland is magmatism associated with the closure of the Iapetus Ocean (Fortey et al., 1996; Neilson et al., 2009; Miles et al., 2014; Corfu et al., 2014; Hines et al., 2018). However, the nearest section of the Iapetus Suture (Fig. 8A) is located ~1200–1400 km from the HCFB and the Bardo Unit, which indicates that only powerful volcanic eruptions could be the source of the tuffites in Poland. Using an analogy with the thickest pyroclastic deposits formed during the Iapetus Ocean closure, such as Kinnekulle K-Bentonite (Upper Ordovician; Bergström et al., 1995) and Osmundsborg K-Bentonite (Silurian–upper Llandovery; Bergström et al., 1998), such a significant distance between the source and depositional areas would cause a gradual increase in the number and thickness of the Polish tuffites towards the west (towards the Iapetus Suture). This means that, equivalents of the Polish tuffites with thicknesses of several or more metres should be deposited in the area of today's western and Central Europe. Explosive volcanic eruptions of such magnitude should therefore be widely recorded at many occurrences of upper Silurian and Lower Devonian successions in those countries. But, the observed lack of such tuffs indicates that the magmatism associated with the closure of Iapetus Ocean was too distant to be the source for the tuffites studied in Poland.

Another region known for the occurrence of late Ludlow and Přídolí volcanic rocks is Podolia in Ukraine and Moldova (Fig. 8A), with numerous K-bentonite layers (Huff et al., 2000; Kipli, 2021). These bentonites were formed during magmatic activity developed over the subduction zone which stretched along the south-eastern margin of the East European Platform (Baltica; Huff et al., 2000; Kipli, 2021; Fig. 8A). The subduction zone continued westwards along the southern margin of Avalonia (Fortey et al., 1996; Franke et al., 2017; Fig. 8A). According to Trela et al. (2018) the same subduction zone supplied volcanic ash to the Silurian K-bentonites in the HCFB. Activity of this zone in the German area was related to late Silurian continental arc magmatism and subsequently Early Devonian back-arc extension in the Rhenohercynian Zone (Fig. 8A) (Zeh and Gerdes, 2010; Zeh and Will, 2010). According to Fortey et al. (1996), Silurian magmatic activity, characterized by a negative europium anomaly, may have taken place along the southern margin of Avalonia (Fig. 8A), which seems to reflect the composition of most of the tuffites analysed from Poland (Fig. 5G). This southern margin of Avalonia/Laurussia is also located very close (up to 200 km) to the outcrops of the tuffites studied (Fig. 8A). The subduction zone along this margin had been probably active since the early Silurian (Winchester et al., 2002b; Will et al., 2018). This indicates that the pyroclastic material deposited during the early and middle Silurian in the HCFB area could have come simultaneously from two different

sources, i.e. from the northwest (closure of the Tornquist Ocean) and the south (southern margin of Avalonia). However, during the late Silurian, pyroclastic material was delivered only from the south. Therefore, the geochemical data from the Niewachłów tuffites, the tuffites from Barcza Mountain and Ždanów were compared with the published geochemical data on upper Silurian and Lower Devonian magmatic rocks probably associated with the southern subduction zone beneath Laurussia. These data fall into two groups. The first comes from the area of the West European Paleozoic Platform (Fig. 8A), which are: Taunus and Lenne (data after von Raumer et al., 2017), Böllsteiner Odenwald (data after Reischmann et al., 2001), the Spessart Crystalline Complex (data after Dombrowski et al., 1995) and the Ruhla Crystalline Complex (data after Brätz, 2000; Appendix 2). The second group is related to pyroclastic rocks occurring on the East European Platform in the Ukraine (Podolia Region) and Moldova (Fig. 8A) (data after Huff et al., 2000; Kipli, 2021; Appendix 2). Harker diagrams of  $\text{Al}_2\text{O}_3$  vs.  $\text{SiO}_2$  (Fig. 9A);  $\text{MgO}$  vs.  $\text{SiO}_2$  (Fig. 9B);  $\text{TiO}_2$  vs.  $\text{SiO}_2$  (Fig. 9C);  $\text{Rb}$  vs.  $\text{SiO}_2$  (Fig. 9D);  $\text{Th/Y}$  vs.  $\text{SiO}_2$  (Fig. 9E) show that the magmatic rocks from each of these locations (including the Polish tuffites) constitute a separate sub-group with a characteristic composition, showing mutual geochemical and geographical affinity. The Harker diagrams indicate that samples from Germany contain more  $\text{SiO}_2$  than the samples from Ukraine (Podolia) and Moldova (Fig. 9). Using  $\text{SiO}_2$  abundance-based diagrams, two collective groups can be distinguished. One group (Fig. 9) represents part of southern Avalonia (Fig. 8A) and largely comprises intrusive rocks from Germany (Dombrowski et al., 1995; Brätz, 2000; Reischmann et al., 2001) that had to be formed in the place of their present occurrence (Fig. 8A); therefore, the pyroclastic rocks (von Raumer et al., 2017) belonging to the same group with similar geochemical composition are probably also of local origin (Fig. 8A). The second group, of Ukrainian (Podolian)-Moldavian bentonites (Fig. 9), was related to the southern active margin of Baltica (Fig. 8A; Huff et al., 2000; Kipli, 2021). Thus, it can be inferred that the source area for the pyroclastic rocks of this group was also local. A unique sub-group are samples of tuffites from Poland (Fig. 8A), which in different diagrams show a variable affiliation to these two groups (Fig. 9A, B, C, E), and in some cases occupy a separate position (Fig. 9D). The geochemical pattern of tuffites from Poland, indicating their partial dissimilarity to the German group and the Ukrainian (Podolian)-Moldavian group (Fig. 9), together with the relatively large thickness of these rocks (Niewachłów tuffites – up to 40 cm, tuffite from Barcza – 150 cm, tuffite from Ždanów – 50 cm; Fig. 2) may mean that their source area was located close to the sedimentary basin. Therefore, the probable source area of the Polish tuffites was associated with the nearest section of the subduction zone, along the southern and south-western margins of the Małopolska Block and the Brunovistulian Block (Fig. 8A).

The  $\text{Th-Zr}/117-\text{Nb}/16$  triangular diagram (Fig. 6B–F) shows that samples from Poland and from all regions compared (except for Böllsteiner Odenwald, with no data) form one coherent group in the Continental Arc Basalt (CAB) field. The tectonic setting indicates the presence of a subduction zone during magma generation for these rocks. The same conclusion holds for the comparison of the geochemical characteristics of the Primitive Mantle-normalized trace elements in samples from these areas (except for Böllsteiner Odenwald, with no data), where small negative anomalies of Nb, Ta (in some samples no data on Ta) and Ti (Fig. 5C–F), corroborating the presence of a subduction zone, are visible. Diagrams of  $\text{Rb}$  vs.  $\text{Y} + \text{Nb}$  and  $\text{Nb}$  vs.  $\text{Y}$  (Fig. 7) yield the greatest comparative possibil-

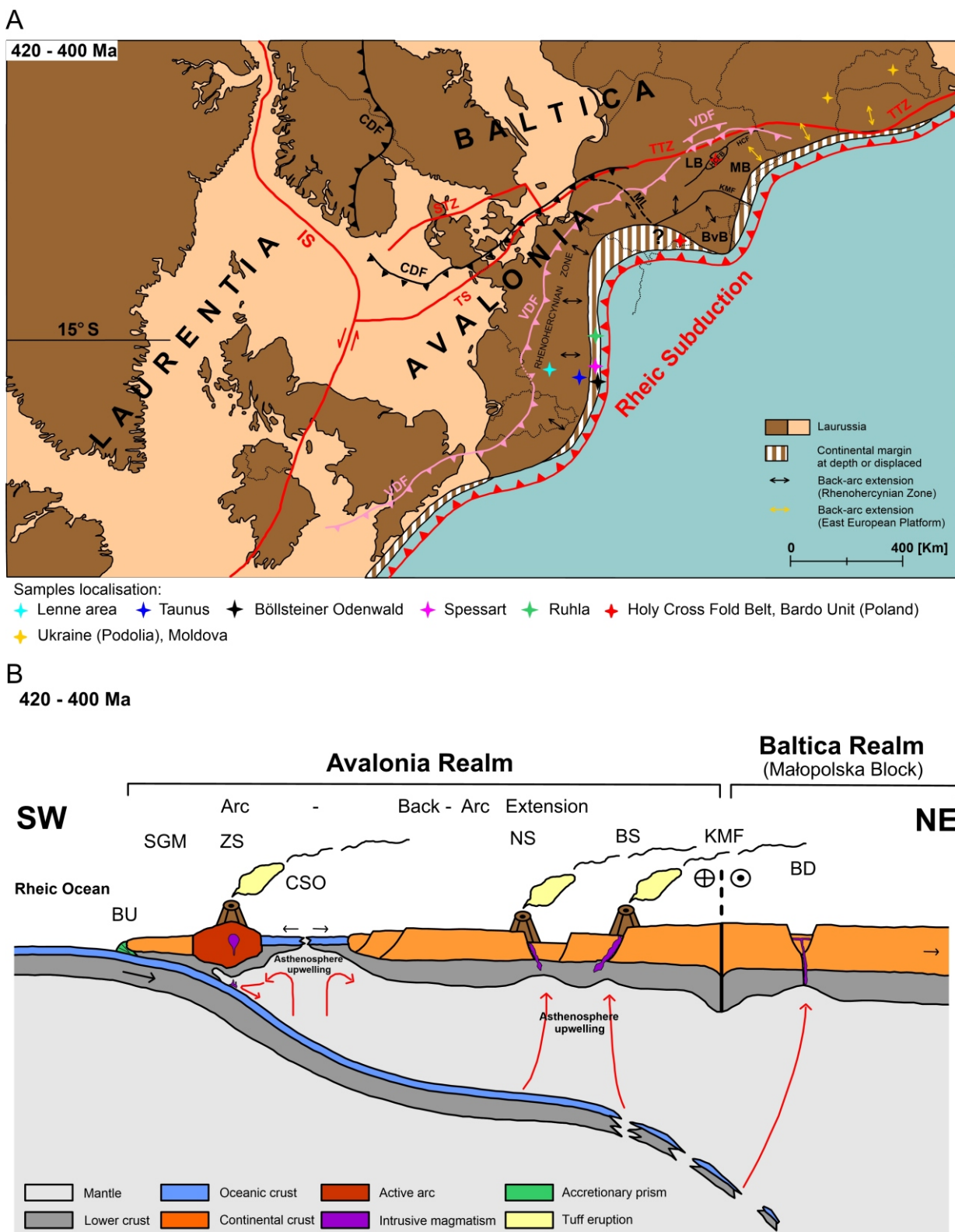
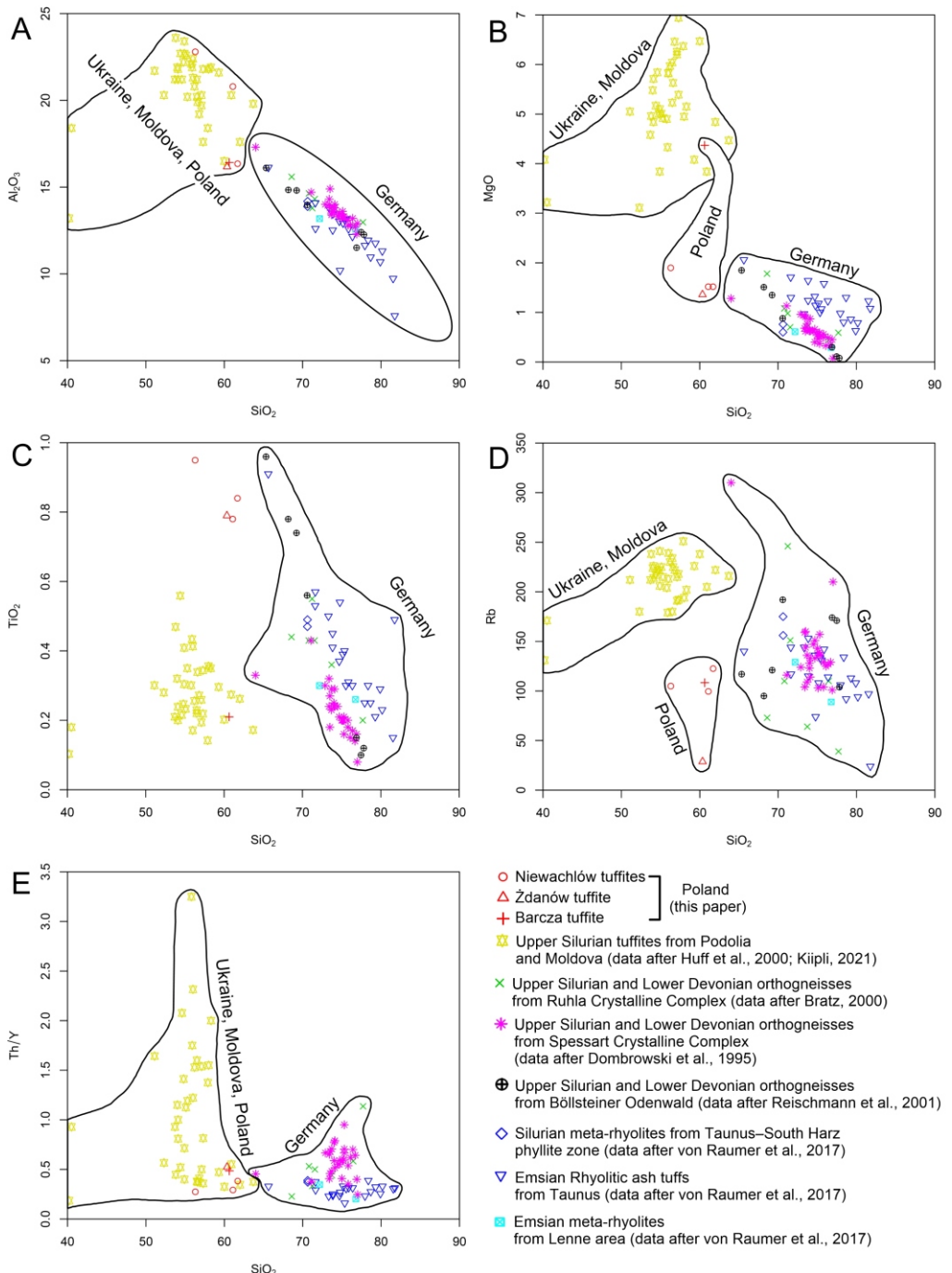


Fig. 8A – late Silurian–Early Devonian palaeogeography of the Laurussia southern margin after docking of Avalonia (after Mazur et al., 2018; supplemented using Fortey et al., 1996; Golonka et al., 2019; Krzywiec et al., 2022, modified), which records the development of rifting in continental back-arc sedimentary basins (e.g., Rhenohercynian Zone), TTZ – Teisseyre–Tornquist Zone, TS – Thor Suture, STZ – Sorgenfrei–Tornquist Zone, IS – Iapetus Suture, CDF – Caledonian Deformation Front, VDF – Variscan Deformation Front (after Mazur et al., 2020), KMF – Kraków–Myszkow Fault Zone (after Brochwicz-Lewiński et al., 1983; Jurewicz, 2018), ML – Northern continuation of the Moravian Line (after Pharaoh et al., 2006), HCF – Holy Cross Fault, HCFB – Holy Cross Fold Belt, LB – Łysogóry Block, MB – Małopolska Block, BvB – Brunovistulian Block; B – conceptual tectonic model of the volcanism investigated along the southern margin of Laurussia during late Silurian–Early Devonian time (close to the contact zone between Avalonian and Baltic crust), BU – Bardo Unit, SGM – Sowie Góry Massif (affinity for the Avalonia after Kröner and Hegner, 1998), CSO – Central Sudetic Ophiolite, KMF – Kraków–Myszków Fault Zone, BD – Bardo Diabase, ZS – Żdanów tuffite Source, NS – Niewachłów Tuffite Source (samples from Czyżów), BS – Barcza tuffite Source

**Fig. 9. Harker diagrams**

**A** –  $\text{SiO}_2$  vs.  $\text{Al}_2\text{O}_3$ ; **B** –  $\text{SiO}_2$  vs.  $\text{MgO}$ ; **C** –  $\text{SiO}_2$  vs.  $\text{TiO}_2$ ; **D** –  $\text{SiO}_2$  vs.  $\text{Rb}$ ; **E** –  $\text{SiO}_2$  vs.  $\text{Th/Y}$

ities, due to the use of data from the largest number of locations (including Böllsteiner Odenwald). On a Rb vs. Y + Nb diagram, points from the all regions compared (Fig. 7) i.e. Taunus, Lenne, Böllsteiner Odenwald, the Spessart Crystalline Complex, the Ruhla Crystalline Complex, Podolia in Ukraine, Moldova and pyroclastic deposits from Poland, plot close to the border between Volcanic Arc Granites (VAG) and Within Plate Granites (WPG), inside the post-collisional setting field. Similarly, in the Nb vs. Y diagram (Fig. 7), all samples form one compact area close to the border of Within Plate Granites (WPG) and the field of Volcanic Arc Granites and syn-Collisional Granites (VAG + syn-COLG).

Compared to the geochemistry of magmatism from the areas considered, rocks from the Taunus and Lenne areas (Figs. 5F, I and 7I, J) and some samples from the Ruhla Crystalline Complex (Figs. 5E, H and 6C, F) are particularly similar to the Polish tuffites. On the other hand, the bentonites from Ukraine and Moldova, despite their close geochemical pattern (Fig. 5C,G) constitute a slightly separate group (Fig. 7K, L), although were formed in a similar tectonic setting (Fig. 6B,F). The pyroclastic rocks from the Taunus and Lenne areas (Fig. 8C) according to von Raumer et al. (2017) were formed from back-arc magmatic activity in the Rhenohercynian Zone. Such classification of the rocks could explain the presence of small negative geochemical anomalies (Nb, Ta; high content of the elements; Fig. 5F) and also the coexistence of these anomalies with the post-collisional regime (Fig. 7I). However, all the samples from Germany, Poland, Ukraine and Moldova indicate their connection with Continental Arc Basalt (CAB; Fig. 6F), consistent with the late Silurian continental arc that stretched along the southern Laurussia margin (Zeh and Gerdes, 2010; Zeh and Will, 2010). Thus, there is an apparent contradiction between the two tectonic regimes; however, according to Gao et al. (2018) and Vasey et al. (2021), the early stage of continental back-arc magmatism usually has signatures similar to arc magmatism. The rocks in question formed in the late Silurian-Early Devonian interval, i.e. at a time when back-arc extension along the southern margin of Laurussia had started (Zeh and Gerdes, 2010; Zeh and Will, 2010; Franke et al., 2017), therefore there is no contradiction between the continental back-arc setting (post-collisional regime) and the Continental Arc Basalt (CAB) signatures. According to Tatsumi et al. (1995), continental back-arc magmatism can be distinguished from continental arc magmatism by the lack of typical magma formed in a subduction zone. This feature is clearly visible in the Nb vs. Zr diagram (Fig. 6A), where almost all samples compared plot in the Back-Arc "Intra-Plate Magmatism" field, which is consistent with the small Nb and Ta anomalies present in them (Fig. 5C-F). On the other hand, some samples from all these regions have greater affinity to an arc setting (Figs. 6A and 7K, L), which probably is related to the stage of evolution of the arc-back-arc system. Simultaneous arc and back-arc magma generation is due to the migration of the magmatic arc front accompanied by lithospheric thinning and incipient rifting, but the contribution of a particular type of volcanism may vary within the same arc depending on the degree of extension (Zagorevski et al., 2010 and cited therein).

Based on the geological context (Fig. 8A) and geochemical composition (Fig. 6A) of the rocks from Poland, Germany, Ukraine and Moldova, it can be concluded that they belong to one large group of magmatic rocks formed at a similar time (late Silurian/Early Devonian) and in a similar tectonic setting, which is the early stage of continental arc-back-arc magmatism on the southern margin of Laurussia (Fig. 8A). During the late Silurian to Late Devonian or early Carboniferous, arc and back-arc magmatic activity associated with the Rhenohercynian Zone

was prevalent in the area of present-day Germany (Zeh and Gerdes, 2010; Zeh and Will, 2010; Eckelmann et al., 2014; von Raumer et al., 2017). Therefore, the upper Silurian and Lower Devonian tuffites from Poland are probably the effect of the initial stage of Rhenohercynian magmatism. Upper Silurian rock samples from Poland and the rest of the regions compared were formed before the Rhenohercynian oceanic crust dated as Emsian (Awdankiewicz et al., 2021); therefore, they are probably the result of pre-rift magmatism during arc-back-arc lithospheric thinning.

#### POLISH TUFFITES AS PART OF ARC-BACK-ARC MAGMATIC ACTIVITY RELATED TO THE RHENOHERCYNIAN ZONE

The results obtained (dating and tectonic setting interpretation) indicate that the volcanic activity associated with the Niewachłów tuffites can be correlated with late Silurian diabase intrusion into the Bardo Syncline in the HCFB (Fig. 1D and Table 1) which formed at a similar time and probably in the same Rhenohercynian back-arc setting (Nawrocki et al., 2020; Fig. 8B). The age of ~433 Ma (Fig. 4D), which is related to inherited zircon cores from the Niewachłów tuffite, can be correlated with the occurrence of numerous bentonites in Telychian and Sheinwoodian strata in northwestern Baltica (Kipli et al., 2013, 2014). This probably corresponded to one of the final stages of the Avalonia-Baltica collision between Llandovery and Wenlock times (De Vos et al., 2010) and indicates that the basement rock, where the Niewachłów tuffite magma was generated, had been previously affected by this collision.

The Niewachłów tuffites in terms of age and mineral association, containing apatite, zircon and monazite (Fig. 3A, B, D), are similar to the Kielce tuff layer (Fig. 1D) in the HCFB, dated by Krzemińska and Krzemiński (2019) at  $414.2 \pm 6.6$  Ma. Despite the large error range in dating the Kielce tuff, from the upper Silurian to Lower Devonian (Krzemińska and Krzemiński, 2019), comparison with biostratigraphic data from the Kielce Beds (Malec, 2001) indicates that the Kielce tuff belongs to upper Silurian rocks (upper Ludlow or younger). This indicates that the Kielce tuff was formed after the end of the volcanic activity located north of the HCFB associated with Avalonia-Baltica collision (Fortey et al., 1996; Kipli et al., 2013, 2014) and can be correlated with the volcanism that took place along the southern margin of the Avalonia-Baltica realm. Therefore the Niewachłów tuffites and Kielce tuff presumably originated from the same magmatic source. Additionally, the volcanic activity in the HCFB area has been documented in middle Ludlow rocks in the Kleczanów PIG1 borehole, where several layers of bentonite were found (Trela et al., 2018) and in the Małacentów 5 borehole where a 0.5 m thick layer of tuffite was described by Dowgiałło (1970). Whereas, in the lower Ludlow graptolitic shales (Pragowiec Beds) in the Bardo Syncline, Langier-Kuźniarowa and Ryka (1972) described 9 layers of K-bentonites containing numerous euhedral biotite crystals and light yellow zircons. Very similar euhedral biotite flakes (Fig. 3C) and pale yellow zircon crystals (Fig. 3D) occur in the Niewachłów tuffites, which may indicate their affinity to the same magmatic source. Furthermore, euhedral biotite crystals with a K-Ar cooling age of  $402.5 \pm 15.2$  Ma were also reported (Kozłowski et al., 2004; Nawrocki et al., 2007) from greywackes of the Niewachłów Beds, which seems to be very close to the age of the Niewachłów tuffites. This means that late Silurian magmatic activity near and in the area of HCFB had not stopped during the greywacke sedimentation. However, at the current stage of research, it is difficult to determine whether the Niewachłów tuffites and greywackes of the Niewachłów Beds come from the same source area. The upper Silurian greywackes in the HCFB

usually contain a few pyroclastic interbeds (Malec, 2001). Fortey et al. (1996), using the example of a similar disappearance of bentonites in an upper Silurian section in the Welsh Borderlands, argued that the preservation of volcanic ash interbeds during the deposition of arenaceous sediments is unlikely. In the case of upper Silurian rocks in the HCFB, the Niewachłów and Kiele Beds mostly consist of siltstones and claystones (Malec, 1993), therefore the type of depositional environment only partially explains less frequency of pyroclastic interbeds. Another explanation for the small number of tuffites and bentonites in these rocks may be the location of the source area. According to Fortey et al. (1996), Huff et al. (2000), Trela et al. (2018) and Kipli (2021), late Silurian volcanic ash beds in the Avalonia-Baltica realm are related to the subduction zone developed along the southern margin of this palaeocontinent. Additionally, Trela et al. (2018) indicated that volcanic ash reached the HCFB region following the direction of the prevailing winds from the southeast. However the prevailing wind direction indicates the dominant transport direction and does not exclude other, if less active, transport directions of the volcanic ash. The wind direction depends on the local system of pressures and temperatures, so it can be variable. An example is the way the radioactive clouds moved during the disaster at the Chernobyl nuclear power plant. According to IAEA (2006), "During the first five days after the accident commenced, the wind pattern had changed through all directions of the compass". Thus, if the source of Niewachłów tuffites had been located in a slightly different place (inconsistent with the dominant wind direction), e.g. south-west of the HCFB, then their transport to this area would have been correspondingly less effective and the number of tuffites would have been lower. This is probably a more complete explanation of the phenomenon.

Despite the incomplete data, all of the late Silurian magmatic rocks noted in the HCFB were formed in a new province of continental arc-back-arc magmatism, extended along the southern margin of Laurussia (Fig. 8A, B). This magmatic activity continued and intensified in the Early Devonian, as indicated by the tectonic setting of the Barcza tuffite (Fig. 6A) and the presence of the entire tuffite succession in the HCFB, described by Tarnowska (1971, 1976). The Silurian–Devonian magmatism in the vicinity of HCFB may be related to the prolongation of the back-arc magmatism to the east from the Rhenohercynian Zone in Germany, which corresponds to the latest interpretation by Nawrocki et al. (2020) for the Bardo diabase in the HCFB.

The back-arc magmatism of the Rhenohercynian Zone continued south-eastwards to the Brunovistulian Block (Kalvoda et al., 2008; Fig. 8A). Its activity already in the Silurian and Early Devonian in the Brunovistulian Block is indicated by the results of isotope dating, made in recent years (Table 1): Velké Vrbno Dome amphibolite  $407.5 \pm 2.5$  Ma (Jastrzębski et al., 2021), granophyre diorite from the Sosnowiec IG 1 borehole  $420 \pm 2$  Ma (Nawrocki et al., 2020), Hlina granite  $430 \pm 6.4$  Ma (Hönig, 2016), basaltic dike from Zelesice  $438 \pm 16$  Ma (Přichystal, 1999). Moreover, according to recent data (Kryza and Pin, 2010; Wojtulek et al., 2017; Awdankiewicz et al., 2021), the Early Devonian Central Sudetic Ophiolite was also formed during seafloor spreading in the back-arc basin. Mazur et al. (2015b) imply that the Central Sudetic Ophiolite was formed on the margin of Avalonia/Bunovistulia. If the link between the Central Sudetic Ophiolite and the Brunovistulian Block is true, then the Central Sudetic Ophiolite may belong to the same continental arc-back-arc zone (Fig. 8B) from which the Polish tuffites originate.

The Ždanów tuffite, which occurs in the graptolitic shales (Přídolí) of the Bardo Unit (Fig. 2), is probably also associated with the margin of Laurussia. The Bardo Unit is an accretionary prism (Franke et al., 1993; Fig. 8B), which, according to Racki et al. (2022) formed along the southern margin of Laurussia. Racki et al. (2022) studied numerous Famennian bentonites in

the Bardo Unit, whose source may be a continental magmatic arc preserved as remnants in the Vrbno Group of the East Sudetes. However, recently Jastrzębski et al. (2021) dated the Velké Vrbno Dome amphibolite at  $407.5 \pm 2.5$  Ma, which indicates that magmatism in this region began much earlier and could be also the origin of the Ždanów tuffite (Přídolí). The origin of the volcanism associated with the Vrbno Group would also explain the greater geochemical affinity of the Ždanów tuffite to a magmatic arc setting (Fig. 8B). However the magmatic arc may also have been destroyed for example during subduction of the Sowie Góry Massif, which according to Tabaud et al. (2021) took place in the Early Devonian ( $\sim 397$ – $402$  Ma; Fig. 8B).

## CONCLUSIONS

The presented studies of pyroclastic rocks in Poland and their comparison with published data on late Silurian-Early Devonian magmatism in related areas in Europe show that:

1. The Niewachłów tuffites, and tuffites from Barcza Mountain and Ždanów formed in a continental arc-back-arc setting during initial extensional magmatism related to the Rhenohercynian Zone.
2. All the areas compared – Taunus, Lenne, Böllsteiner Odenwald, the Spessart Crystalline Complex, the Ruhla Crystalline Complex, Podolia in Ukraine, Moldova and the Polish tuffites – reflect the same setting of late Silurian and Early Devonian continental arc-back-arc magmatism, probably associated with the same magmatic province. The upper Silurian rocks may be correlated with the pre-rift magmatism stage in the Rhenohercynian zone.
3. U-Pb dating of the Niewachłów tuffites yielded an age of  $419.91 \pm 1.7$  Ma, corresponding to the late Silurian (Přídolí). This indicates that part of the greywacke section in the Bardo Syncline, previously classified as Ludlow, may be younger and belong to the Přídolí.
4. In and around the HCFB area, magmatic activity did not stop in the upper Silurian, but continued at least to the Lower Devonian. It was associated with the new magmatic province, developing from the late Silurian at the southern margin of Laurussia.

Further investigations are necessary to expand knowledge concerning the nature of late Silurian–Early Devonian magmatism in the HCFB, including geochemical and isotopic analyses of zircons.

**Acknowledgements.** The research was supported with funds from the Statutory Activity of the DSM 2016 No 113222, DSM 2017 No 115620 Faculty of Geology, University of Warsaw. I am grateful to R. Anczkiewicz for performing zircon U-Pb dating of the Niewachłów tuffite and M. Kusiak for enabling analyzes of the geochemical composition of two rock samples. I would like to thank E. Jurewicz for her numerous insightful comments and explanations during the preparation of the entire manuscript, K. Nejbert for detailed and patient discussion on the geotectonic setting of the formation of the studied rocks and P. Jokubauskas for lots of advice regarding calculations and interpretation of the results of geochemical analyzes and U-Pb dating, without which this work would not have been written. I sincerely thank to W. Kozłowski for introducing me to the Silurian geology of the Holy Cross Mountains during preparation of my master's thesis. I would like to express my gratitude to the both anonymous reviewers for a number of insightful comments that significantly improved the content of the manuscript. I am indebted to T. Peryt for editorial handling and J. Zalasiewicz for English proofreading.

## REFERENCES

- Anczkiewicz, A.A., Anczkiewicz, R., 2016.** U-Pb zircon geochronology and anomalous Sr-Nd-Hf isotope systematics of late orogenic andesites: Pieniny Klippen Belt, Western Carpathians, South Poland. *Chemical Geology*, **427**: 1–16; <https://doi.org/10.1016/j.chemgeo.2016.02.004>
- Anczkiewicz, R., Porębski, S.J., Kędzior, A., Paszkowski, M., 2017.** Geochronologia i tektonogeneza ordowicko-sylurskich K-bentonitów basenu bałtyckiego (in Polish). In: Opracowanie map zasięgu, biostratygrafia utwórzów dolnego paleozoiku oraz analiza ewolucji tektonicznej przykrawędziowej strefy platformy wschodnioeuropejskiej dla oceny rozmieszczenia niekonwencjonalnych złóż węglowodorów (eds. J. Golonka and S. Bębenek): 306–319. Wydawnictwo Arka, Cieszyn.
- Arculus, R.J., Powell, R., 1986.** Source component mixing in the regions of arc magma generation. *Journal of Geophysical Research: Solid Earth*, **91**: 5913–5926; <https://doi.org/10.1029/JB091iB06p05913>
- Awdankiewicz, M., Kryza, R., Turniak, K., Ovtcharova, M., Schaltegger, U., 2021.** The Central Sudetic Ophiolite (European Variscan Belt): precise U-Pb zircon dating and geotectonic implications. *Geological Magazine*, **158**: 555–566; <https://doi.org/10.1017/S0016756820000722>
- Barret, T.J., Jarvis, I., Jarvis, K.E., 1990.** Rare earth element geochemistry of massive sulfides-sulfates and gossans on the Southern Explorer Ridge. *Geology*, **18**: 583–586; [https://doi.org/10.1130/0091-7613\(1990\)018<0583:REEGOM>2.3.CO;2](https://doi.org/10.1130/0091-7613(1990)018<0583:REEGOM>2.3.CO;2)
- Batchelor, R.A., Jeppsson, L., 1999.** Wenlock metabentonites from Gotland, Sweden: geochemistry, sources and potential as chemostratigraphic markers. *Geological Magazine*, **136**: 661–669; <https://doi.org/10.1017/S001675689900285X>
- Bełka, Z., Valverde-Vaquero, P., Dörr, W., Ahrendt, H., Wemmer, K., Franke, W., 2002.** Accretion of first Gondwana-derived terranes at the margin of Baltica. *Geological Society Special Publications*, **201**: 19–36; <https://doi.org/10.1144/GSL.SP.2002.201.01.02>
- Bergström, S.M., Huff, W.D., Kolata, D.R., Bauert, H., 1995.** Nomenclature, stratigraphy, chemical fingerprinting, and areal distribution of some Middle Ordovician K-bentonites in Baltoscandia. *GFF*, **117**: 1–13; <https://doi.org/10.1080/11035899509546191>
- Bergström, S.M., Huff, W.D., Kolata, D.R., 1998.** The Lower Silurian Osmundsberg K-bentonite. Part I: Stratigraphic position, distribution, and palaeogeographic significance. *Geological Magazine*, **135**: 1–13; <https://doi.org/10.1017/S0016756897007887>
- Berthelsen, A., 1992.** From Precambrian to Variscan Europe. In: *A Continent Revealed – the European Geotraverse* (eds. D.J. Blundell, R. Freeman and S. Mueller): 153–164. Cambridge University Press, Cambridge; <https://doi.org/10.1017/CBO9780511608261>
- Berthelsen, A., 1998.** The Tornquist Zone northwest of the Carpathians: An intraplate pseudosuture. *GFF*, **120**: 223–230; <https://doi.org/10.1080/11035899801202223>
- Brätz, H., 2000.** Radiometrische Altersdatierungen und geochemischen Untersuchungen von Orthogneisen, Granite und Granitporphyren aus dem Ruhlaer Kristallin, Mitteldeutsche Kristallinzone. Ph.D. thesis, Universität Würzburg; <https://nbn-resolving.org/urn:nbn:de:bvb:20-opus-2320>
- Brochwicz-Lewiński, W., Pożaryski, W., Tomczyk, H., 1983.** Palaeozoic strike-slip movements in Southern Poland (in Polish with English summary). *Przegląd Geologiczny*, **31**: 651–658.
- Chorowska, M., 1990.** The Silurian and Devonian deposits in the southern part of the Bardo Structure - the Sudety Mts (in Polish with English summary). *Kwartalnik Geologiczny*, **34** (3): 411–432.
- Corfu, F., Andersen, T.B., Gasser, D., 2014.** The Scandinavian Caledonides: main features, conceptual advances and critical questions. *Geological Society Special Publications*, **390**: 9–43; <https://doi.org/10.1144/SP390.25>
- Czarnocki, J., 1919.** Stratygrafia i tektonika Gór Świętokrzyskich (in Polish). *Prace Towarzystwa Naukowego Warszawskiego*, **28**: 1–172.
- Czarnocki, J., 1936.** Überblick der Stratigraphie und Paläogeographie des Unterdevons im Polnischen Mittelgebirge (in Polish with German summary). *Sprawozdania Państwowego Instytutu Geologicznego*, **8**: 1–27.
- Czarnocki, J., 1939.** Field work in the Święty Krzyż Mountains in 1938 (in Polish with English summary). *Biuletyn Państwowego Instytutu Geologicznego*, **15**: 1–27.
- Czarnocki, J., 1957.** Tectonics of the Święty Krzyż Mountains. Geology of the Łysogóry Region (in Polish with English summary). *Prace Instytutu Geologicznego*, **18**: 11–138.
- Dadlez, R., Kowalczewski, Z., Znosko, J., 1994.** Some key problems of the pre-Permian tectonics of Poland. *Geological Quarterly*, **38** (2): 169–190.
- De Vos, W., Feldrappe, H., Pharaoh, T.C., Smith, N.J.P., Vejbak, O.V., Verniers, J., Nawrocki, J., Poprawa, P., Bełka, Z., 2010.** Pre-Devonian. In: *Petroleum Geological Atlas of the Southern Permian Basin Area* (eds. J.C. Doornenbal and A.G. Stevenson): 59–69. EAGE Publications b.v. (Houten); <http://hdl.handle.net/1854/LU-1002680>
- Dombrowski, A., Henjes-Kunst, F., Höhndorf, A., Kröner, A., Okrusch, M., Richter, P., 1995.** Orthogneisses in the Spessart Crystalline Complex, Northwest Bavaria: Silurian granitoid magmatism at an active continental margin. *Geologische Rundschau*, **84**: 399–411; <https://doi.org/10.1007/BF00260449>
- Douville, E., Bienvenu, P., Charlou, J.L., Donva, J.P., Fouquet, Y., Appriou, P., Gamo, T., 1999.** Yttrium and rare earth elements in fluids from various deep-sea hydrothermal systems. *Geochimica et Cosmochimica Acta*, **63**: 627–643; [https://doi.org/10.1016/S0016-7037\(99\)00024-1](https://doi.org/10.1016/S0016-7037(99)00024-1)
- Dowgiałło, W.D., 1970.** Wyniki wierceń geologicznych wykonanych w Paśmie Bielińskim i Wale Małacentowskim w Górach Świętokrzyskich (in Polish). *Kwartalnik Geologiczny*, **14** (4): 924–925.
- Eckelmann, K., Nesbo, H.D., Königshof, P., Linnemann, U., Hofmann, M., Lange, J.M., Sagawe, A., 2014.** Plate interactions of Laurussia and Gondwana during the formation of Pangaea—Constraints from U-Pb LA-SF-ICP-MS detrital zircon ages of Devonian and Early Carboniferous siliciclastics of the Rhenohercynian zone, Central European Variscides. *Gondwana Research*, **25**: 1484–1500; <https://doi.org/10.1016/j.gr.2013.05.018>
- Elliott, T., 2003.** Tracers of the slab. *Geophysical Monograph Series*, **138**: 23–45; <https://doi.org/10.1029/138GM03>
- Fijałkowska-Mader, A., Malec, J., 2018.** Age of the Lower Devonian tuffite horizon from Barcza (in Polish with English summary). *Przegląd Geologiczny*, **66**: 578–584; <http://doi.org/10.7306/2018.8>
- Fortey, N., Merriman, R., Huff, W., 1996.** Silurian and late Ordovician K-bentonites as a record of late Caledonian volcanism in the British Isles. *Earth and Environmental Science Transactions of the Royal Society of Edinburgh*, **86**: 167–180; <https://doi.org/10.1017/S0263593300002212>
- Franke, W., Cocks, L.R.M., Torsvik, T.H., 2017.** The Paleozoic Variscan oceans revisited. *Gondwana Research*, **48**: 257–284; <https://doi.org/10.1016/j.gr.2017.03.005>
- Franke, W., Żelaźniewicz, A., Porębski, S.J., Wajsprych, B., 1993.** Saxothuringian Zone in Germany and Poland: differences and common features. *Geologische Rundschau*, **82**: 583–599; <https://doi.org/10.1007/BF00212418>
- Gao, Z., Zhang, H.-R., Yang, H., Pan, F.-B., Luo, B.-J., Guo, L., Xu, W.-C., Tao, L., Zhang, L.-Q., Wu, J., 2018.** Back-arc basin development: Constraints on geochronology and geochemistry of arc-like and OIB-like basalts in the Central Qilian block (Northwest China). *Lithos*, **310–311**: 255–268; <https://doi.org/10.1016/j.lithos.2018.04.002>
- Gągała, Ł., 2015.** Late Silurian deformation in the Łysogóry Region of the Holy Cross Mountains revisited: restoration of a progressive Caledonian unconformity in the Klonów Anticline and its im-

- plications for the kinematics of the Holy Cross Fault (central Poland). *Geological Quarterly*, **59** (3): 441–456; <https://doi.org/10.7306/gq.1222>
- Golonka, J., Porębski, S. J., Barmuta, J., Papiernik, B., Bębenek, S., Barmuta, M., Botor, D., Pietsch, K., Słomka, T., 2019.** Palaeozoic palaeogeography of the East European Craton (Poland) in the framework of global plate tectonics. *Annales Societatis Geologorum Poloniae*, **89**: 381–403; <https://doi.org/10.14241/asgp.2019.16>
- Grad, M., Janik, T., Yliniemi, J., Guterch, A., Luosto, U., Tiira, T., Komminaho, K., Oeroda, P., Höing, K., Makris, J., Lund, C.E., 1999.** Crustal structure of the Mid-Polish Trough beneath the Teisseyre-Tornquist Zone seismic profile. *Tectonophysics*, **314**: 145–160; [https://doi.org/10.1016/S0040-1951\(99\)00241-3](https://doi.org/10.1016/S0040-1951(99)00241-3)
- Grad, M., Guterch, A., Mazur, S., Keller, G.R., Špičák, A., Hrubcová, P., Geissler, W.H., 2008.** Lithospheric structure of the Bohemian Massif and adjacent Variscan belt in central Europe based on profile S01 from the SUDETES 2003 experiment. *Journal of Geophysical Research*, **113**: 1–25; <https://doi.org/10.1029/2007JB005497>
- Gravunder, A., Merten, D., Büchel, G., 2014.** Origin of middle rare earth element enrichment in acid mine drainage-impacted areas. *Environmental Science and Pollution Research*, **21**: 812–823; <https://doi.org/10.1007/s11356-013-2107-x>
- Hastie, A.R., Kerr, A.C., Pearce, J.A., Mitchell, S.F., 2007.** Classification of altered volcanic island arc rocks using immobile trace elements: Development of the Th-Co discrimination diagram. *Journal of Petrology*, **48**: 2341–2357; <https://doi.org/10.1093/petrology/egm062>
- Hines, R., Paterson, S.R., Memeti, V., Chambers, J.A., 2018.** Nested incremental growth of zoned upper crustal plutons in the Southern Uplands Terrane, UK: Fractionating, mixing, and contaminated magma fingers. *Journal of Petrology*, **59**: 483–516; <https://doi.org/10.1093/petrology/egy034>
- Hofmann, A.W., 1997.** Mantle geochemistry: the message from oceanic volcanism. *Nature*, **385**: 219–229; <https://doi.org/10.1038/385219a0>
- Hönig, S., 2016.** Hlina granitic suite: 430 Ma felsic layered granit-bearing magma portion of bimodal, back-arc related magmatism, SW Brunovistulicum – a multidisciplinary study. Ph.D. thesis; Mášářkova univerzita; <https://is.muni.cz/th/fty6l/>
- Huff, W.D., Bergström, S.M., Kolata, D.R., 2000.** Silurian K-bentonites of the Dnestr Basin, Podolia, Ukraine. *Journal of the Geological Society*, **157**: 493–504; <https://doi.org/10.1144/jgs.157.2.493>
- IAEA, 2006.** Environmental Consequences of the Chernobyl Accident and their Remediation: Twenty Years of Experience. Report of the Chernobyl Forum Expert Group 'Environment'. Radiological Assessment Reports Series, **8**: 21–22.
- Janoušek, V., Farrow, C.M., Erban, V., 2006.** Interpretation of whole-rock geochemical data in igneous geochemistry: introducing geochemical data toolkit (GCDkit). *Journal of Petrology*, **47**: 1255–1259; <https://doi.org/10.1093/petrology/egi013>
- Jastrzębski, M., Żelaźniewicz, A., Sláma, J., Machowiak, K., Śliwiński, M., Jaźwa, A., Kocjan, I., 2021.** Provenance of Precambrian basement of the Brunovistulian Terrane: new data from its Silesian part (Czech Republic, Poland), central Europe, and implications for Gondwana break-up. *Precambrian Research*, **355**: 106108; <https://doi.org/10.1016/j.precamres.2021.106108>
- Jurewicz, E., 2018.** The Šariš Transitional Zone, revealing interactions between Pieniny Klippen Belt, Outer Carpathians and European platform. *Swiss Journal of Geosciences*, **111**: 245–267; <https://doi.org/10.1007/s00015-017-0297-9>
- Kalvoda, J., Babek, O., Fatka, O., Leichmann, J., Melichar, R., Nehyba, S., Spacek, P., 2008.** Brunovistulian terrane (Bohemian Massif, Central Europe) from late Proterozoic to late Paleozoic: a review. *International Journal of Earth Sciences*, **97**: 497–518; <https://doi.org/10.1007/s00531-007-0183-1>
- Kardymowicz, I., 1960a.** Tuffite from Barcza Mountain near Zagnańsk (Święty Krzyż Mountains) (in Polish with English summary). *Kwartalnik Geologiczny*, **4** (3): 597–608.
- Kardymowicz, I., 1960b.** Celadonite from Barcza in the Święty Krzyż Mountains (in Polish with English summary). *Kwartalnik Geologiczny*, **4** (3): 609–618.
- Kiipli, T., 2021.** Silurian volcanism recorded in sedimentary sections at the southwestern margin of the East European Platform: geochemical correlation and tectono-magmatic interpretation. *Geological Quarterly*, **65** (1): 1–8; <https://doi.org/10.7306/gq.1580>
- Kiipli, T., Kallaste, T., Kiipli, E., Radževičius, S., 2013.** Correlation of Silurian bentonites based on the immobile elements in the East Baltic and Scandinavia. *GFF*, **135**: 152–161; <https://doi.org/10.1080/11035897.2013.783104>
- Kiipli, T., Radževičius, S., Kallaste, T., 2014.** Silurian bentonites in Lithuania: correlations based on sanidine phenocryst composition and graptolite biozonation – interpretation of volcanic source regions. *Estonian Journal of Earth Sciences*, **63**: 18–29; <https://doi.org/10.3176/earth.2014.02>
- Konon, A., 2008.** Tectonic subdivision of Poland: Holy Cross Mountains and adjacent areas (in Polish with English summary). *Przegląd Geologiczny*, **56**: 921–926.
- Kowalczewski, Z., Lisik, R., 1974.** New data on diabases and geological structure of the Pragowiec area in the Góry Świętokrzyskie Mts (in Polish with English summary). *Bulletin Instytutu Geologicznego*, **275**: 113–158.
- Kozłowski, W., Tomczykowa, E., 1999.** A new occurrence of benthic fauna in the Niewachłów Greywackes (Upper Silurian) from Zalesie near Łagów in the Holy Cross Mountains. *Geologica Quarterly*, **43** (1): 129–126.
- Kozłowski, W., Domańska, J., Nawrocki, J., Pecsak, Z., 2004.** The provenance of the Upper Silurian greywackes from the Holy Cross Mountains (Central Poland). *Mineralogical Society of Poland, Special Papers*, **24**: 251–254.
- Kozłowski, W., Domańska-Siuda, J., Nawrocki, J., 2014.** Geochemistry and petrology of the upper Silurian greywackes from the Holy Cross Mountains (Central Poland): implications for the Caledonian history of the southern part of the Trans-European Suture Zone (TESZ). *Geological Quarterly*, **58** (2): 311–336; <https://doi.org/10.7306/gq.1160>
- Kremer, B., 2006.** Mat-forming coccoid cyanobacteria from early Silurian marine deposits of Sudetes, Poland. *Acta Palaeontologica Polonica*, **51**: 143–154.
- Kröner, A., Hegner, E., 1998.** Geochemistry, single zircon ages and Sm-Nd systematics of granitoid rocks from the Góra Sowie (Owl Mts), Polish West Sudetes: evidence for early Palaeozoic arc-related plutonism. *Journal of the Geological Society*, **155**: 711–724; <https://doi.org/10.1144/gsjgs.155.4.0711>
- Kryza, R., Pin, C., 2010.** The Central-Sudetic ophiolites (SW Poland): petrogenetic issues, geochronology and palaeotectonic implications. *Gondwana Research*, **17**: 292–305; <https://doi.org/10.1016/j.gr.2009.11.001>
- Kryza, R., Muszer, J., Haydukiewicz, J., August, C., Jurasić, M., Rodionov, N., 2011.** A SIMS zircon age for a biostratigraphically dated Upper Viséan (Asbian) bentonite in the Central-European Variscides (Bardo Unit, Polish Sudetes). *International Journal of Earth Sciences*, **100**: 1227–1235; <https://doi.org/10.1007/s00531-010-0529-y>
- Krzemiński, L., 2004.** Geochemical constraints on the origin of the mid-Palaeozoic diabases from the Holy Cross Mts. and Upper Silesia, southeastern Poland. *Geological Quarterly*, **48** (2): 147–158.
- Krzemińska, E., Krzemiński, L., 2019.** Magmatic episodes in the Holy Cross Mountains, Poland - a new contribution from multi-age zircon populations. *Bulletin Państwowego Instytutu Geologicznego*, **474**: 43–58; <https://doi.org/10.5604/01.3001.0013.0839>
- Krzywiec, P., Kufrasa, M., Poprawa, P., Mazur, S., Koperska, M., Ślęmp, P., 2022.** Together but separate: decoupled Variscan (late Carboniferous) and Alpine (Late Cretaceous-Paleogene) inversion tectonics in NW Poland. *Solid Earth*, **13**: 639–658; <https://doi.org/10.5194/se-13-639-2022>
- Lamarche, J., Lewandowski, M., Mansy, J.L., Szulczeński, M., 2003.** Partitioning pre-, syn- and post Variscan deformation in the Holy Cross Mountains, eastern Variscan foreland. *Geological Society Special Publications*, **208**: 159–184; <https://doi.org/10.1144/GSL.SP.2003.208.01.08>
- Langier-Kuñiarowa, A., Ryka, W., 1972.** Silurian bentonites of the Góry Świętokrzyskie Mountains (in Polish with English summary). *Bulletin Instytutu Geologicznego*, **261**: 7–30.

- Li, W., Ge, C., Wang, F., Sun, H., Gu, H., 2021.** The spatial distribution characteristics of Nb-Ta of mafic rocks in subduction zones. *Open Geosciences*, **13**: 390–400; <https://doi.org/10.1515/geo-2020-0242>
- Liu, H., Li, Y., Wu, L., Huangfu, P., Zhang, M., 2018.** Geochemistry of high-Nb basalt-andesite in the Erguna Massif (NE China) and implications for the early Cretaceous back-arc extension. *Geological Journal*, **54**: 291–307; <https://doi.org/10.1002/gj.3176>
- Malec, J., 1991.** "Szarogłazy niewachłowskie" w profilu górnego syluru regionu południowego Gór Świętokrzyskich (in Polish). *Kwartalnik Geologiczny*, **35** (2): 284–285.
- Malec, J., 1993.** Upper Silurian and Lower Devonian in the western Holy Cross Mts. *Geological Quarterly*, **37** (4): 501–536.
- Malec, J., 2000.** Wstępne dane o przeobrażeniach termicznych materii organicznej w szarogłazach górnego syluru Góra Świętokrzyskich (in Polish). Posiedzenia Naukowe Państwowego Instytutu Geologicznego, **56**: 109–111.
- Malec, J., 2001.** Sedimentology of deposits around the Late Caldonian unconformity in the western Holy Cross Mountains. *Geological Quarterly*, **45** (4): 397–415.
- Malec, J., 2006.** Sylur w Górách Świętokrzyskich (in Polish). In: Procesy i zdarzenia w historii geologicznej Góra Świętokrzyskich (eds. S. Skompski and A. Żylińska): 36–50. LXVII Zjazd Naukowy Polskiego Towarzystwa Geologicznego, Ameliówka k. Kielc, 28–30 czerwca 2006 r. Polskie Towarzystwo Geologiczne, Państwowy Instytut Geologiczny, Wydział Geologii Uniwersytetu Warszawskiego.
- Malec, J., 2014.** Stratigraphical position of the Widelki Formation in the Bardo Syncline (Holy Cross Mts.) (in Polish with English summary). *Przegląd Geologiczny*, **62**: 748–754.
- Malec, J., Kuleta, M., Migaszewski, Z., 2016.** Lithologic-petrographic characterization of Silurian rocks in the Niestachów profile (Holy Cross Mountains). *Annales Societatis Geologorum Poloniae*, **86**: 85–110; <https://doi.org/10.14241/asgp.2015.017>
- Mazur, S., Aleksandrowski, P., Kryza, R., Oberc-Dziedzic, T., 2006.** The Variscan Orogen in Poland. *Geological Quarterly*, **50** (1): 89–118.
- Mazur, S., Mikolajczak, M., Krzywiec, P., Malinowski, M., Buffenmyer, V., Lewandowski, M., 2015a.** Is the Teisseyre-Tornquist Zone an ancient plate boundary of Baltica? *Tectonics*, **34**: 2465–2477; <https://doi.org/10.1002/2015TC003934>
- Mazur, S., Turniak, K., Szczepański, J., McNaughton, N.J., 2015b.** Vestiges of Saxothuringian crust in the Central Sudetes, Bohemian Massif: Zircon evidence of a recycled subducted slab provenance. *Gondwana Research*, **27**: 825–839; <https://doi.org/10.1016/j.gr.2013.11.005>
- Mazur, S., Porębski, S.J., Kędzior, A., Paszkowski, M., Podhalńska, T., Poprawa, P., 2018.** Refined timing and kinematics for Baltica-Avalon convergence based on the sedimentary record of a foreland basin. *Terra Nova*, **30**: 8–16; <https://doi.org/10.1111/ter.12302>
- Mazur, S., Aleksandrowski, P., Gągała, Ł., Krzywiec, P., Żaba, J., Gaidzik, K., Sikora, R., 2020.** Late Palaeozoic strike-slip tectonics versus oroclininal bending at the SW outskirts of Baltica: case of the Variscan belt's eastern end in Poland. *International Journal of Earth Sciences*, **109**: 1133–1160; <https://doi.org/10.1007/s00531-019-01814-7>
- Mazur, S., Malinowski, M., Maystrenko, Y.P., Gągała, Ł., 2021.** Pre-existing lithospheric weak zone and its impact on continental rifting - The Mid-Polish Trough, Central European Basin System. *Global and Planetary Change*, **198** (103417); <https://doi.org/10.1016/j.gloplacha.2021.103417>
- McDonough, W.F., Sun, S.-S., 1995.** The composition of the Earth. *Chemical Geology*, **120**: 223–253; [https://doi.org/10.1016/0009-2541\(94\)00140-4](https://doi.org/10.1016/0009-2541(94)00140-4)
- Migaszewski, Z.M., Gałuszka, A., Dolegowska, S., 2016.** Rare earth and trace element signatures for assessing an impact of rock mining and processing on the environment: Wiśniówka case study, south-central Poland. *Environmental Science and Pollution Research*, **23**: 24943–24959; <https://doi.org/10.1007/s11356-016-7713-y>
- Miles, A., Graham, C., Hawkesworth, C., Gillespie, M., Dhuime, B., Hinton, R., 2014.** Using zircon isotope compositions to constrain crustal structure and pluton evolution: the Iapetus Suture Zone granites in northern Britain. *Journal of Petrology*, **55**: 181–207; <https://doi.org/10.1093/petrology/egt065>
- Modliński, Z., Szymański, B., 2001.** The Silurian of the Nida, Holy Cross Mts. and Radom areas, Poland – a review. *Geological Quarterly*, **45** (4): 435–454.
- Nakamura, N., 1974.** Determination of REE, Ba, Fe, Mg, Na and K in carbonaceous and ordinary chondrites. *Geochimica et Cosmochimica Acta*, **38**: 757–775; [https://doi.org/10.1016/0016-7037\(74\)90149-5](https://doi.org/10.1016/0016-7037(74)90149-5)
- Narkiewicz, M., Petecki, Z., 2017.** Basement structure of the Paleozoic Platform in Poland. *Geological Quarterly*, **61** (2): 502–520; <https://doi.org/10.7306/gq.1356>
- Narkiewicz M., Maksym, A., Malinowski, M., Grad, M., Guerch, A., Petecki, Z., Probulski, J., Janik, T., Majdański, M., Środa, P., Czuba, W., Gaczyński, E., Jankowski, L., 2015.** Transcurrent nature of the Teisseyre-Tornquist Zone in Central Europe: results of the POLCRUST-01 deep reflection seismic profile. *International Journal of Earth Sciences*, **104**: 775–796; <https://doi.org/10.1007/s00531-014-1116-4>
- Nawrocki, J., Poprawa, P., 2006.** Development of Trans-European Suture Zone in Poland: from Ediacaran rifting to Early Palaeozoic accretion. *Geological Quarterly*, **50** (1): 59–76.
- Nawrocki, J., Dunlap, J., Pecska, Z., Krzeminski, L., Żylińska, A., Fanning, M., Kozłowski, W., Salwa, S., Szczepaniak, Z., Trela, W., 2007a.** Late Neoproterozoic to Early Palaeozoic palaeogeography of the Holy Cross Mountains (Central Europe): an integrated approach. *Journal of the Geological Society*, **164**: 405–423; <https://doi.org/10.1144/0016-76492006-023>
- Nawrocki, J., Polechońska, O., Salwa, S., 2007b.** Spatial model of the Bardo intrusion in the vicinity of Zagórze (Kielce region of the Holy Cross Mts) in the light of a new magnetic survey (in Polish with English summary). *Przegląd Geologiczny*, **55**: 1136–1142.
- Nawrocki, J., Salwa, S., Pańczyk, M., 2013.** New  $^{40}\text{Ar}$ - $^{39}\text{Ar}$  age constraints for magmatic and hydrothermal activity in the Holy Cross Mts. (southern Poland). *Geological Quarterly*, **57** (3): 551–60; <https://doi.org/10.7306/gq.1117>
- Nawrocki, J., Pańczyk, M., Szrek, P., 2020.** Magmatic activity at the Silurian/Devonian boundary in the Brunovistula and Małopolska Terranes (S Poland): Possible link with the Rheic Ocean closure and the onset of the Rheno-Hercynian Basin. *Geological Magazine*, **157**: 119–133; <https://doi.org/10.1017/S0016756819000384>
- Neilson, J.C., Kokelaar, B.P., Crowley, Q.G., 2009.** Timing, relations and cause of plutonic and volcanic activity of the Siluro-Devonian post-collision magmatic episode in the Grampian Terrane, Scotland. *Journal of the Geological Society*, **166**: 545–561; <https://doi.org/10.1144/0016-76492008-069>
- Obst, K., Böhnke, A., Katzung, G., Maletz, J., 2002.** Pb-Pb zircon dating of tuff horizons in the Cyrtograptus Shale (Wenlock, Silurian) of Bornholm, Denmark. *Bulletin of the Geological Society of Denmark*, **49**: 1–8; <https://doi.org/10.3757/bgsd-2003-49-01>
- Pearce, J.A., 1996.** Sources and settings of granitic rocks. *Episodes*, **19**: 120–125; <https://doi.org/10.18814/epiugs/1996/v19i4/005>
- Pearce, J.A., Harris, N.B.W., Tindle, A.G., 1984.** Trace element discrimination diagrams for the tectonic interpretation of granitic rocks. *Journal of Petrology*, **25**: 956–983; <https://doi.org/10.1093/petrology/25.4.956>
- Pharaoh, T.C., 1999.** Palaeozoic terranes and their lithospheric boundaries within the Trans-European Suture Zone (TESZ): a review. *Tectonophysics*, **314**: 17–41; [https://doi.org/10.1016/S0040-1951\(99\)00235-8](https://doi.org/10.1016/S0040-1951(99)00235-8)
- Pharaoh, T.C., Winchester, J.A., Verniers, J., Lasse, A., Seghedi, A., 2006.** The western accretionary margin of the east European craton: an overview. *Geological Society Memoirs*, **32**: 291–311; <https://doi.org/10.1144/GSL.MEM.2006.032.01.17>
- Porębska, E., 1982.** Latest Silurian and Early Devonian graptolites from Źdanów section, Bardo Mts. (Sudetes). *Annales Societatis Geologorum Poloniae*, **52**: 89–209.
- Porębska, E., Sawłowicz, Z., 1997.** Palaeoceanographic linkage of geochemical and graptolite events across the Silurian-Devonian boundary in Bardzkie Mountains (Southwest Poland). *Palaeogeography, Palaeoclimatology, Palaeoecology*, **132**: 343–354; [https://doi.org/10.1016/S0031-0182\(97\)00048-5](https://doi.org/10.1016/S0031-0182(97)00048-5)

- Přichystal, A., 1999.** K-Ar age determination of a basaltic dike from Zelesice (Brno massif) (in Czech with English summary). *Geologické výzkumy na Moravě a ve Slezsku*, **6**: 120–121.
- Racki, G., 2006.** Zarys stratygrafii (in Polish). In: Procesy i zdarzenia w historii geologicznej Górz Świętokrzyskich (eds. S. Skompski and A. Źlińska): 51–55. LXXVII Zjazd Naukowy Polskiego Towarzystwa Geologicznego, Ameliówka, Guide-book.
- Racki, G., Mazur, S., Narkiewicz, K., Pisarzowska, A., Bardziński, W., Koltonik, K., Szymanowski, D., Filipiak, P., Kremer, B., 2022.** Awaning Saxothuringian Ocean evidenced in the Famennian tephra-bearing biosiliceous succession of Bardo Unit (Central Sudetes, SW Poland). *GSA Bulletin*, **134**: 1–26; <https://doi.org/10.1130/B35971.1>
- Reischmann, T., Anthes, G., Jaeckel, P., Altenberger, U., 2001.** Age and origin of the Böllsteiner Odenwald. *Mineralogy and Petrology*, **72**: 29–44; <https://doi.org/10.1007/s007100170025>
- Smit, J., van Wees, J.-D., Cloetingh, S., 2016.** The Thor suture zone: from subduction to intraplate basin setting. *Geology*, **44**: 707–710; <https://doi.org/10.1130/G37958.1>
- Stupnicka, E., 1995.** Fazy ruchów tektonicznych w górnym sylurze i dolnym dewonie w południowej części Górz Świętokrzyskich (in Polish). *Przegląd Geologiczny*, **43**: 110–112.
- Stupnicka, E., Przybyłowicz, T., Żbikowska, B., 1991.** Age of the Niewachłów greywackes and shales from Widęki near Bardo (Holy Cross Mts) (in Polish with English summary). *Przegląd Geologiczny*, **39**: 389–393.
- Tabaud, A.S., Štípká, P., Mazur, S., Schulmann, K., Míková, J., Wong, J., Sun, M., 2021.** Evolution of a Cambro-Ordovician active margin in northern Gondwana: Geochemical and zircon geochronological evidence from the Góry Sowie metasedimentary rocks, Poland. *Gondwana Research*, **90**: 1–26; <https://doi.org/10.1016/j.gr.2020.10.011>
- Tarnowska, M., 1971.** Lower Devonian polymict and tufaceous rocks in the Kielce Region of the Świętokrzyskie Mountains (in Polish with English summary). *Kwartalnik Geologiczny*, **15** (3): 569–597.
- Tarnowska, M., 1976.** Lithological correlation of the Lower Devonian in the eastern part of the Górz Świętokrzyskie (in Polish with English abstract). *Bulletin Instytutu Geologicznego*, **296**: 75–128.
- Tatsumi, Y., Kogiso, T., Nohda, S., 1995.** Formation of a third volcanic chain in Kamchatka: generation of unusual subduction-related magmas. *Contributions to Mineralogy and Petrology*, **120**: 117–128; <https://doi.org/10.1007/BF00287109>
- Tomczyk, H., 1962.** Stratigraphic problems of the Ordovician and Silurian in Poland in the light of recent studies (in Polish with English summary). *Prace Instytutu Geologicznego*, **35**: 1–134.
- Tomczykowa, E., Tomczyk, H., 1981.** Rozwój badań syluru I najniższego dewonu w Górzach Świętokrzyskich (In Polish). In: Przewodnik 53 Zjazdu Polskiego Towarzystwa Geologicznego, Kielce 6–8 września 1981 (ed. H. Żakowa): 42–57. Wyd. Geol., Warszawa.
- Trela, W., Bąk, E., Pańczyk, M., 2018.** Upper Ordovician and Silurian ash beds in the Holy Cross Mountains, Poland: preservation in mudrock facies and relation to atmospheric circulation in the Southern Hemisphere. *Journal of the Geological Society*, **175**: 352–360; <https://doi.org/10.1144/jgs2017-026>
- Torsvik, T.H., Rehnström, E.F., 2003.** The Tornquist Sea and Baltica-Avalonia docking. *Tectonophysics*, **362**: 67–82; [https://doi.org/10.1016/S0040-1951\(02\)00631-5](https://doi.org/10.1016/S0040-1951(02)00631-5)
- Vasey, D.A., Cowgill, E., Cooper, K.M., 2021.** A preliminary framework for magmatism in modern continental back-arc basins and its application to the Triassic-Jurassic tectonic evolution of the Caucasus. *Geochemistry, Geophysics, Geosystems*, **22**; <https://doi.org/10.1029/2020GC009490>
- Vermeesch, P., 2018.** IsoplotR: a free and open toolbox for geo-chronology. *Geoscience Frontiers*, **9**: 1479–1493; <https://doi.org/10.1016/j.gsf.2018.04.001>
- von Raumer, J.F., Nesbor, H.-D., Stampfli, G.M., 2017.** The north-subducting Rheic Ocean during the Devonian: consequences for the Rhenohercynian ore sites. *International Journal of Earth Sciences*, **106**: 2279–2296; <https://doi.org/10.1007/s00531-016-1425-x>
- Wajsprych, B., 1978.** Allochthonous Paleozoic rocks in the Visean of the Bardzkie Mts., Sudetes (in Polish with English summary). *Annales de la société géologique de Pologne*, **48**: 99–127.
- Walczak, A., Bełka, Z., 2017.** Fingerprinting Gondwana versus Baltica provenance: Na and Sr isotopes in Lower Paleozoic clastic rocks of the Małopolska and Łysogóry terranes, southern Poland. *Gondwana Research*, **45**: 138–151; <https://doi.org/10.1016/j.gr.2017.02.002>
- Will, T.M., Schmädicke, E., Ling, X.-X., Li, X.-H., Li, Q.-L., 2018.** New evidence for an old idea: Geochronological constraints for a paired metamorphic belt in the central European Variscides. *Lithos*, **302–303**: 278–297; <https://doi.org/10.1016/j.lithos.2018.01.008>
- Winchester, J.A., Floyd, P.A., 1977.** Geochemical discrimination of different magma series and their differentiation products using immobile elements. *Chemical Geology*, **20**: 325–343; [https://doi.org/10.1016/0009-2541\(77\)90057-2](https://doi.org/10.1016/0009-2541(77)90057-2)
- Winchester, J.A., and the PACE TMR Network Team 2002a.** Palaeozoic amalgamation of Central Europe: new results from recent geological and geophysical investigations. *Tectonophysics*, **360**: 5–21; [https://doi.org/10.1016/S0040-1951\(02\)00344-X](https://doi.org/10.1016/S0040-1951(02)00344-X)
- Winchester, J.A., Pharaoh, T.C., Verniers, J., 2002b.** Palaeozoic amalgamation of Central Europe: an introduction and synthesis of new results from recent geological and geophysical investigations. *Geological Society Special Publications*, **201**: 1–18; <https://doi.org/10.1144/gsl.sp.2002.201.01.01>
- Winchester, J.A., Pharaoh, T.C., Verniers, J., Ioane, D., Seghedi, A., 2006.** Palaeozoic accretion of Gondwana-derived terranes to the East European Craton: recognition of detached terrane fragments dispersed after collision with promontories. *Geological Society Memoirs*, **32**: 323–332; <https://doi.org/10.1144/GSL.MEM.2006.032.01.19>
- Wojtulek, P.M., Puziewicz, J., Ntaflos, T., 2017.** MORB melt metasomatism and deserpentinization in the peridotitic member of Variscan ophiolite: an example of the Braszowice-Brzeźnica serpentinites (SW Poland). *Journal of Geosciences*, **62**: 147–164; <https://doi.org/10.3190/jgeosci.240>
- Wood, D.A., 1980.** The application of a Th-Hf-Ta diagram to problems of tectonomagmatic classification and to establishing the nature of crustal contamination of basaltic lavas of the British Tertiary volcanic province. *Earth Planetary Science Letters*, **50**: 11–30; [https://doi.org/10.1016/0012-821X\(80\)90116-8](https://doi.org/10.1016/0012-821X(80)90116-8)
- Wójcik, E., Pelc, A., Pacek, A., 2021.** Late Variscan deformation events in the Bardo Syncline revealed by biotite K-Ar dating of Ludlow-age tuffite (Holy Cross Mountains, Poland). *Geological Quarterly*, **65** (1): 1–19; <https://doi.org/10.7306/gq.1586>
- Wyżga, B., 1987.** Lower Palaeozoic of the Bardo Mountains (Sudetes): a sequence of deep-sea pelagic sediments (in Polish with English summary). *Geologica Sudetica*, **22**: 119–145.
- Zagorevski, A., van Staal, C.R., Rogers, N., McNicoll, V.J., Pollock, J., 2010.** Middle Cambrian to Ordovician arc-backarc development on the leading edge of Ganderia, Newfoundland Appalachians. *GSA Memoir*, **206**: 1–30; [https://doi.org/10.1130/2010.1206\(16\)](https://doi.org/10.1130/2010.1206(16))
- Zeh, A., Gerdes, A., 2010.** Baltica- and Gondwana-derived sediments in the Mid-German Crystalline Rise (Central Europe): implications for the closure of the Rheic ocean. *Gondwana Research*, **17**: 254–263; <https://doi.org/10.1016/j.gr.2009.08.004>
- Zeh, A., Will, T.M., 2010.** The mid-German Crystalline Zone. In: Pre-Mesozoic Geology of Saxon-Thuringia (eds. U. Linnemann and R.L. Romer): 195–220. Schweizerbart, Stuttgart.
- Żelaźniewicz, A., Buła, Z., Fanning, M., Seghedi, A., Żaba, J., 2009.** More evidence on Neoproterozoic terranes in Southern Poland and south eastern Romania. *Geological Quarterly*, **53** (1): 93–124.
- Żelaźniewicz, A., Oberc-Dziedzic, T., Sláma, J., 2020.** Baltica and the Cadomian orogen in the Ediacaran-Cambrian: a perspective from SE Poland. *International Journal of Earth Sciences*, **109**: 1503–1528; <https://doi.org/10.1007/s00531-020-01858-0>

**APPENDIX 1**  
**The in situ U-Pb (La ICP-MS) zircon dating analysis of T1 layer of Niewachłów tuffites**

Grain spot	207Pb / 235U	± 2SE	206Pb / 238U	± 2SE	U238 / 206Pb	±2SE	207Pb / 206Pb	± 2SE	Age 207Pb / 235U	± 2SE	Age 206Pb / 238U	± 2SE	Age 207Pb / 206Pb	±2SE
The analysis of homogeneous zircons and external crystal growth zones selected to calculate the concordia age														
T1a - 1	0.545	0.046	0.0675	0.0013	14.81481	0.2853224	0.0592	0.0051	428	30	420.6	8.1	350	170
T1a - 2	0.537	0.04	0.0679	0.0012	14.72754	0.2602805	0.0572	0.0043	429	26	423.2	7.3	390	150
T1a - 3	0.493	0.034	0.0672	0.0011	14.88095	0.243587	0.0536	0.0038	398	23	419.1	6.5	230	140
T1a - 5	0.524	0.023	0.06757	0.00079	14.79947	0.1730291	0.0563	0.0024	425	15	421.5	4.8	420	95
T1a - 6	0.514	0.023	0.06655	0.00082	15.0263	0.1851474	0.0561	0.0026	418	15	415.3	4.9	398	100
T1a - 8	0.532	0.048	0.068	0.0015	14.70588	0.3243945	0.0579	0.0056	418	33	423.7	9	270	180
T1a - 9	0.528	0.036	0.068	0.0013	14.70588	0.2811419	0.0563	0.0038	423	24	423.7	7.9	350	140
T1a - 10	0.542	0.05	0.0674	0.0018	14.8368	0.3962349	0.0595	0.0057	421	33	420	11	320	190
T1a - 11	0.513	0.06	0.0683	0.0017	14.64129	0.3644245	0.0558	0.0063	410	39	425	10	200	210
T1b - 3	0.535	0.031	0.06721	0.00098	14.87874	0.2169493	0.0578	0.0034	428	21	419.2	5.9	410	130
T1c - 5	0.505	0.039	0.067	0.001	14.92537	0.2227668	0.0551	0.0041	410	25	417.7	6.3	300	140
T1c - 13	0.526	0.032	0.06802	0.0011	14.70156	0.2377494	0.0558	0.0034	423	22	424.1	6.5	350	130
T1c - 14	0.518	0.027	0.0676	0.0009	14.7929	0.1969469	0.0567	0.0031	422	19	421.9	5.4	390	110
T1c - 1	0.537	0.16	0.0675	0.0018	14.81481	0.3950617	0.0586	0.012	430	59	421	11	460	170
The youngest excluded analyse														
T1a - 12	0.527	0.03	0.0658	0.0011	15.19757	0.2540627	0.0582	0.0034	426	20	410.8	6.4	480	120
The analysis of inherited zircon cores														
T1a - 4	0.529	0.027	0.0676	0.00099	14.7929	0.2166416	0.0574	0.003	425	19	421.9	6	410	110
T1a - 7	0.561	0.06	0.0696	0.0018	14.36782	0.3715815	0.0602	0.0066	427	40	433	11	270	210
T1a - 13	0.535	0.035	0.0685	0.0011	14.59854	0.2344291	0.0569	0.0036	429	23	427.3	6.4	390	130
T1b - 1	0.529	0.035	0.0696	0.0012	14.36782	0.247721	0.0552	0.0037	424	23	433.6	7.3	310	140
T1b - 2	0.494	0.038	0.0696	0.0013	14.36782	0.2683644	0.0524	0.004	405	26	433.7	7.6	210	150
T1b - 4	0.523	0.031	0.06781	0.001	14.74709	0.2174766	0.056	0.0033	420	20	422.8	6.2	350	120
T1b - 5	0.508	0.055	0.0689	0.0017	14.51379	0.3581051	0.0538	0.0059	393	37	429.4	10	110	210
T1b - 8	0.521	0.028	0.06952	0.00099	14.38435	0.2048404	0.0547	0.003	426	19	433.2	5.9	340	120
T1d - 1	0.516	0.031	0.0683	0.0011	14.64129	0.2358041	0.0551	0.0033	413	21	426	6.4	310	130
T1d - 2	0.553	0.032	0.0695	0.0011	14.38849	0.2277315	0.0577	0.0031	441	21	433.2	6.3	430	120
T1c - 2	0.527	0.031	0.06927	0.00091	14.43626	0.1896492	0.0556	0.0031	426	19	431.7	5.5	350	110
T1c - 3	0.519	0.03	0.0713	0.0012	14.02525	0.236049	0.0533	0.0031	420	20	444	7.2	260	120
T1c - 4	0.571	0.037	0.07	0.0012	14.28571	0.244898	0.0608	0.0043	453	23	435.9	7.2	530	130
T1c - 9	0.518	0.047	0.0706	0.0017	14.16431	0.3410669	0.0537	0.005	407	33	439.2	10	160	180
T1c - 11	0.597	0.03	0.07215	0.0011	13.86001	0.21131	0.0603	0.0031	473	20	449	6.4	530	110
T1c - 12	0.504	0.035	0.0695	0.0012	14.38849	0.2484343	0.0533	0.0038	407	24	432.8	7.2	210	140
T1c - 10	0.533	0.33	0.0709	0.0034	14.10437	0.6763733	0.0567	0.02	430	92	441.6	20	400	210
T1c - 8	0.845	0.13	0.07	0.0019	14.28571	0.3877551	0.0895	0.011	604	53	436	11	1170	170

## APPENDIX 2

## Major and trace element geochemistry of Upper Silurian and Lower Devonian samples from Germany, Ukraine (Podolia) and Moldova

Author Sample	Bratz 2000 93002	Bratz 2000 93007	Bratz 2000 93010	Bratz 2000 93015	Bratz 2000 93025	Bratz 2000 96005	Raumer et al. 2017 45,358	Raumer et al. 2017 45,357	Raumer et al. 2017 46,282	Raumer et al. 2017 46,281	Raumer et al. 2017 46,280	Raumer et al. 2017 46,278	Raumer et al. 2017 46,277	Raumer et al. 2017 46,276	Raumer et al. 2017 46,275	Raumer et al. 2017 46,274	Raumer et al. 2017 46,273	Raumer et al. 2017 46,271	Raumer et al. 2017 46,270	Raumer et al. 2017 46,269	Raumer et al. 2017 46,268	Raumer et al. 2017 46,266	Raumer et al. 2017 46,265	Raumer et al. 2017 46,264		
Major oxides (wt %)																										
SiO <sub>2</sub>	73.72	70.80	71.23	76.44	68.60	71.55	77.70	70.63	70.64	73.84	78.37	79.91	75.86	80.17	78.68	81.55	76.37	79.29	74.78	75.54	65.64	81.76	74.69	77.95	75.36	
Al <sub>2</sub> O <sub>3</sub>	13.74	14.64	13.79	12.77	15.59	14.31	12.97	13.88	14.18	12.52	11.93	10.69	12.59	11.31	10.96	9.73	12.15	11.76	10.19	13.17	16.13	7.58	13.03	11.63	13.12	
Fe <sub>2</sub> O <sub>3</sub> T	2.18*	2.92*	4.34*	1.46*	3.19*	2.74*	1.56	3.38	3.37	4.37	2.05	2.09	2.81	1.81	2.46	2.17	2.65	2.05	4.35	2.56	6.17	4.27	3.18	2.58	2.82	
CaO	1.86	1.93	1.22	0.69	1.82	0.45	2.48	1.15	0.65	0.08	0.02	0.04	0.03	0.02	0.27	0.02	0.41	0.01	1.60	0.03	0.18	0.15	0.07	0.01	0.06	
MgO	0.71	1.08	0.98	0.44	1.78	0.70	0.59	0.60	0.76	1.64	0.80	0.63	1.58	0.79	1.30	1.23	0.86	1.14	1.07	2.06	1.08	1.32	0.98	1.00		
Na <sub>2</sub> O	4.16	3.63	2.80	3.58	4.65	3.31	3.76	3.21	3.56	0.75	0.25	0.78	0.57	0.34	0.69	0.08	1.00	0.36	1.56	1.32	1.60	1.89	1.67	1.68	1.20	
K <sub>2</sub> O	1.60	4.12	4.84	4.19	2.95	4.10	1.08	4.41	3.85	2.58	3.03	2.45	3.16	2.55	2.19	2.27	2.64	2.56	1.71	2.84	3.09	0.52	2.74	2.29	3.02	
MnO	0.03	0.05	0.06	0.02	0.06	0.02	0.06	0.05	0.05	0.06	0.06	0.12	0.03	0.06	0.05	0.03	0.07	0.04	0.11	0.05	0.07	0.06	0.11	0.04		
TiO <sub>2</sub>	0.36	0.43	0.55	0.17	0.44	0.43	0.20	0.47	0.49	0.45	0.30	0.29	0.31	0.23	0.25	0.15	0.30	0.21	0.54	0.30	0.91	0.49	0.37	0.25	0.40	
P <sub>2</sub> O <sub>5</sub>	0.06	0.11	0.13	0.04	0.09	0.11	0.02	0.13	0.14	0.08	0.04	0.05	0.03	0.03	0.03	0.02	0.04	0.02	0.09	0.04	0.19	0.11	0.05	0.03	0.04	
* value recalculated to Fe <sub>2</sub> O <sub>3</sub> T																										
Trace elements (ppm)																										
Ba	436	1791	523	717	733	594	240	807	815	332	383	310	598	345	463	382	568	506	483	425	403	73	380	295	881	
Be																										
Co	31.0	22.0	24.0	<10.0	39.0	41.0	<10.0	7.0	7.0	8.0	4.0	5.0	4.0	2.0	4.0	2.0	5.0	2.0	12.0	4.0	14.0	10.0	7.0	4.0	4.0	
Cs																										
Ga	12.0	20.0	22.0	15.0	19.0	14.0	14.0	16.0	17.0	18.0	18.0	20.0	19.0	16.0	14.0	17.0	19.0	13.0	19.0	20.0	9.0	18.0	16.0	21.0		
Hf																										
Nb	16.0	6.0	17.0	12.0	7.0	15.0	<5.0	17.0	21.0	22.0	21.0	20.0	25.0	20.0	18.0	22.0	27.0	22.0	12.0	23.0	22.0	12.0	23.0	22.0		
Rb	64.0	110.0	246.0	110.0	73.0	151.0	39.0	175.0	156.0	115.0	134.0	108.0	142.0	94.0	92.0	114.0	113.0	113.0	131.0	140.0	136.0	106.0	133.0			
Sn	<15.0	<15.0	<15.0	<15.0	<15.0	<15.0	<15.0	<15.0	<15.0	<15.0	<15.0	<15.0	<15.0	<15.0	<15.0	<15.0	<15.0	<15.0	<15.0	<15.0	<15.0	<15.0	<15.0	<15.0		
Sr	98.0	567.0	192.0	93.0	364.0	79.0	341.0	86.0	64.0	30.0	21.0	25.0	24.0	46.0	42.0	18.0	38.0	61.0	42.0	34.0	51.0	43.0	39.0	33.0	29.0	
Ta																										
Th	15.0	<5.0	18.0	7.0	<5.0	13.0	<5.0	17.91	18.50	13.80	15.90	12.50	18.90	16.80	14.30	16.00	19.30	7.53	17.80	13.50	8.78	16.20	15.00	17.00		
U	<5.0	<5.0	<5.0	<5.0	<5.0	<5.0	<5.0	2.75	2.94	3.17	3.26	2.49	3.97	3.25	3.13	2.61	3.44	3.33	1.60	3.84	2.99	1.74	3.47	2.81	3.82	
V	31.0	48.0	46.0	27.0	69.0	56.0	32.0	39.0	43.0	50.0	28.0	24.0	23.0	15.0	23.0	11.0	28.0	13.0	64.0	31.0	113.0	51.0	40.0	23.0	26.0	
Zr	198.0	166.0	361.0	107.0	149.0	174.0	130.0	220.0	231.0	229.0	214.0	247.0	293.0	291.0	201.0	160.0	234.0	269.0	179.0	218.0	289.0	391.0	217.0	214.0	464.0	
Y	34.0	4.7	54.0	12.0	11.0	26.0	2.2	46.0	50.0	58.0	41.0	49.0	60.0	51.0	52.0	47.0	51.0	60.0	28.0	58.0	41.0	28.0	69.0	65.0	65.0	
La	46.0	43.0	49.0	29.0	42.0	11																				



Dombrowski et al. 1995 Sp91-14	Dombrowski et al. 1995 Sp91-15	Dombrowski et al. 1995 Sp91-16	Dombrowski et al. 1995 Sp91-19	Dombrowski et al. 1995 Sp-1/1	Dombrowski et al. 1995 Sp-1/2	Dombrowski et al. 1995 Sp-1/3	Dombrowski et al. 1995 Sp-2/1	Dombrowski et al. 1995 Sp-3/1	Dombrowski et al. 1995 Sp-3/2a	Dombrowski et al. 1995 Sp-3/2b	Dombrowski et al. 1995 Sp-5/1	Dombrowski et al. 1995 Sp-6/1	Dombrowski et al. 1995 Sp-6/2	Dombrowski et al. 1995 Sp-7/1	Dombrowski et al. 1995 Sp-8/1	Reischmann et al. 2001 Bol-01	Reischmann et al. 2001 Bol-02	Reischmann et al. 2001 Bol-03	
75.80	75.30	75.20	71.10	73.70	74.10	64.00	76.40	73.40	77.00	74.70	73.50	75.80	76.90	73.70	74.50	70.59	77.48	69.24	
13.10	13.20	13.30	14.70	13.40	14.00	17.30	13.20	14.30	12.90	13.50	14.90	12.80	12.30	13.50	13.30	13.98	12.40	14.81	
1.46*	1.50*	1.72*	2.92*	2.14*	2.29*	2.59*	1.58*	1.87*	0.96*	1.65*	1.71*	1.55*	1.36*	2.31*	2.05*	3.42	0.96	4.30	
1.02	1.04	1.03	1.71	1.47	1.56	0.43	0.84	1.06	0.52	1.27	1.71	1.17	1.05	1.76	1.35	1.49	0.62	2.32	
0.56	0.59	0.56	1.13	0.69	0.87	1.28	0.49	0.68	0.07	0.40	0.62	0.50	0.45	0.77	0.61	0.88	0.11	1.35	
4.00	3.66	4.02	4.19	4.03	4.28	2.88	3.44	4.00	3.16	4.09	3.92	3.64	3.58	4.06	3.76	2.79	3.30	4.16	
3.49	4.15	3.67	3.43	3.55	2.56	9.70	3.82	4.06	5.67	3.29	3.43	3.51	3.80	2.57	3.70	5.10	4.79	2.29	
0.03	0.04	0.03	0.07	0.06	0.06	0.06	0.02	0.04	0.02	0.03	0.06	0.03	0.04	0.04	0.04	0.06	0.04	0.09	
0.20	0.20	0.20	0.43	0.23	0.29	0.33	0.17	0.24	0.08	0.21	0.18	0.18	0.16	0.29	0.24	0.56	0.10	0.74	
0.05	0.05	0.04	0.11	0.04	0.08	0.10	0.05	0.08	0.04	0.06	0.09	0.04	0.04	0.09	0.08	0.15	0.02	0.17	
674	692	698	685	680	590	1540	760	620	300	660	720	1010	910	500	670	795	452	396	
14.0	13.0	13.0	20.0														16.0	14.0	18.0
14.0	13.0	13.0	17.0	17.0	17.0	21.0	12.0	17.0	23.0	17.0	15.0	12.0	13.0	15.0	18.0	17.0	14.0	19.0	
129.0	157.0	139.0	116.0	136.0	114.0	310.0	127.0	159.0	210.0	151.0	160.0	104.0	101.0	109.0	147.0	192.0	171.0	121.0	
95.0	103.0	98.0	151.0	150.0	185.0	145.0	105.0	96.0	60.0	92.0	240.0	135.0	100.0	150.0	125.0	83.0	35.0	143.0	
14.00	16.00	15.00	12.00	13.00	16.00	15.00	7.00	13.00	13.00	16.00	11.00	13.00	14.00	12.00	16.00				
22.0	28.0	23.0	40.0	24.0	30.0	33.0	16.0	25.0	7.0	21.0	15.0	16.0	12.0	32.0	22.0	45.0	61.0		
98.0	105.0	103.0	174.0	90.0	108.0	139.0	69.0	106.0	<50.0	109.0	80.0	82.0	87.0	96.0	98.0	229.0	80.0	255.0	
26.0	24.0	25.0	32.0	27.0	31.0	33.0	10.0	32.0	53.0	29.0	24.0	37.0	35.0	17.0	29.0	34.0	30.0	29.0	
35.00	49.00	53.00	<10.00		76.0	75.0	75.0	71.0	75.0	68.0	67.0	54.0	76.0	75.0	64.0	76.0			
22.0	16.0	13.0	22.0	25.0	23.0	33.0	13.0	8.0	27.0	13.0	15.0	32.0	29.0	10.0	30.0		22.0	7.0	
19.0	19.0	23.0	<10.0	64.0	35.0	36.0	24.0	26.0	<20.0	25.0	32.0	32.0	28.0	33.0	36.0	52.0	68.0		
<10.0					27.0	19.0	22.0	14.0	7.0	9.0	6.0	<1.0	8.0	5.0	30.0	11.0	10.0		

Reischmann et al. 2001 Bol-04	Reischmann et al. 2001 Bel-05	Reischmann et al. 2001 Bol-06	Reischmann et al. 2001 Bol-09	Huff et al. 2000 C10	Huff et al. 2000 C6	Huff et al. 2000 M7	Huff et al. 2000 C3-1	Huff et al. 2000 C3-2	Kipli 2021 Kishinjov – 1, Depth 517.0m	Kipli 2021 Pidhaytsi – 1, Depth 1090.0m	Kipli 2021 Pidhaytsi – 1, Depth 1090.0m	Kipli 2021 Vilhovets – 6, Depth 138.0m	Kipli 2021 Horodok – 9, Depth 390.0m	Kipli 2021 Ustya – 7, Depth 131.0m	Kipli 2021 Trybchyn – 65, exposure	Kipli 2021 Trybchyn – 65, exposure	Kipli 2021 Trybchyn – 64, exposure	Kipli 2021 Zavadivka – 6, Depth 1249.5m	Kipli 2021 Kudryntsi – 166, exposure	
77.82	68.18	76.89	65.35	40.50	55.30	52.30	53.70	54.10	56.50	54.80	55.10	56.20	63.70	54.10	40.20	56.00	57.90	54.90	54.90	
12.26	14.84	11.51	16.10	18.40	20.20	20.30	21.20	21.80	21.20	22.20	22.60	20.80	19.80	21.20	13.20	22.40	18.40	23.40	22.70	
0.72	4.78	1.86	6.39	3.63	0.97	3.17	1.44	1.19	1.13	2.33	1.75	1.46	1.44	1.97	0.74	1.06	1.33	2.29	2.29	
0.48	1.95	0.44	2.59	12.6	0.64	2.45	1.05	0.55	0.77	0.18	0.17	0.51	0.18	1.23	19.46	0.35	1.64	0.37	0.55	
0.08	1.51	0.30	1.85	3.22	4.92	3.11	4.58	4.84	5.23	5.00	5.01	5.97	4.47	5.71	4.08	5.83	6.37	3.84	5.10	
2.91	4.50	1.88	3.47	0.01	0.01	0.05	0.06	0.02												
5.16	2.18	6.40	3.05	6.11	8.89	8.88	7.41	7.76	8.55	8.10	8.38	8.18	6.61	7.79	6.10	7.78	7.80	7.33	8.18	
0.02	0.09	0.04	0.10						0.003	0.005	0.005	0.006	0.003	0.009	0.003	0.003	0.003	0.005	0.006	
0.12	0.78	0.15	0.96	0.18	0.35	0.28	0.21	0.20	0.22	0.247	0.233	0.256	0.172	0.239	0.103	0.171	0.142	0.304	0.409	
0.02	0.21	0.10	0.13	0.01	0.10	0.03	0.04	0.03	0.07	0.06	0.06	0.11	0.07	0.06	0.06	0.04	0.03	0.07	0.10	
149	468	356	792	120 2.0	130 3.0	260 2.0	190 2.0	140 3.0	68	184	198	153	70	105	82	140	124	320	149	
10.0	18.0	14.0	21.0	15.9 8.0	12.8 11.0	15.5 12.0	16.3 12.0	15.0 26.0		28.0	27.0	29.0	23.0	27.0	14.0	26.0	22.0	27.0	19.0	
6.0	18.0 95.0	18.0 174.0	9.0 117.0	19.0 171.0	18.0 215.0	25.0 180.0	27.0 212.0	31.0 214.0	29.0 180.0	34.0 222.0	31.0 225.0	28.0 230.0	17.0 216.0	19.0 226.0	13.0 131.0	22.0 239.0	17.0 251.0	20.0 241.0	23.0 206.0	
74.0	158.0	54.0	165.0	66.0 2.2	35.0 1.8	45.0 2.9	52.0 2.2	47.0 2.6	50.0	152.0	141.0	47.0	172.0	109.0	104.0	21.0	26.0	170.0	341.0	
59.0 80.0	283.0 29.0	83.0 26.0	283.0 26.0	130.0 14.0	260.0 26.0	210.0 30.0	230.0 28.0	162.0 10.0	171.0 17.0	157.0 16.0	162.0 16.0	125.0 40.0	150.0 21.0	94.0 18.0	145.0 46.0	115.0 16.0	144.0 45.0	251.0 21.0		
16.0				7.30 16.9	12.60 31.7	25.70 53.2	22.50 44.9	22.70 46.1	14.00 <15.0	28.00 18.0	<15.00 17.0	33.00 22.00	22.00 46.00	46.00 49.0	36.00 24.0	22.00 48.0	15.00 38.0	43.00 30.0	18.00 51.0	66.0
11.0	57.0 11.0	22.0 20.0	87.0	5.1 43.0	8.9 8.0	4.8 4.0	3.1 2.0	12.6 <10.0		12.0 <10.0	12.0 <10.0	12.0 <10.0	<10.0 <10.0	<10.0 <10.0	<10.0 <10.0	<10.0 <10.0	10.0 9.0	<10.0 9.0		
				12.0 14.0	8.3 3.0	15.0 7.0	16.0 9.0	11.0 6.0	15.0 23.0	17.0 25.0	14.0 11.0	15.0 8.0	17.0 6.0	10.0 8.0	9.0 3.0	9.0 4.0	19.0 26.0	20.0 18.0		
				0.6 1.6 0.5 0.5	0.3 0.5 0.8 0.7	0.8 0.4 0.4 0.4	0.4 0.4 0.8 0.2	0.8 1.3 1.6 0.6	7.0 7.0 16.0 1.6	7.0 7.0 3.6 3.6	7.0 7.0 1.3 1.3	12.0 12.0 3.0 3.0	6.0 6.0 5.0 5.0	6.0 6.0 3.0 3.0	6.0 6.0 2.0 2.0	6.0 6.0 3.0 3.0	10.0 9.0 9.0 9.0	<10.0 9.0 9.0 9.0		
				1.5 1.5	0.6 0.6	1.6 1.6	1.6 1.6	0.7 0.7	0.7 0.7	0.7 0.7	0.7 0.7	0.7 0.7	0.7 0.7	0.7 0.7	0.7 0.7	0.7 0.7	3.0 3.0	8.0 8.0		

Kipli 2021 Pidhaytsi – 1, Depth 1143.6m	Kipli 2021 Okopy-Bilivtsi – 46, exposure	Kipli 2021 Pidhaytsi – 1, Depth 1144.6m	Kipli 2021 Zavadivka – 1, Depth 1364.0m	Kipli 2021 Pryhorodok – 117, exposure	Kipli 2021 Pryhorodok – 107, exposure	Kipli 2021 Pidhaytsi – 1, Depth 1148.3m	Kipli 2021 Zavadivka – 6, Depth 1281.5m	Kipli 2021 Vilhovets – 6, Depth 183.0m	Kipli 2021 Kishinjov – 1, Depth 553.5m	Kipli 2021 Zavadivka – 6, Depth 1289.3m	Kipli 2021 Kishinjov – 1, Depth 560.5m	Kipli 2021 Pidhaytsi – 1, Depth 1188.0m	Kipli 2021 Bernove-Okopy – 5, Depth 48.6m	Kipli 2021 Ustyia – 7, Depth 281.0m	Kipli 2021 Vilhovets – 6, Depth 248.0m
54.00	55.80	54.60	53.80	58.30	58.00	54.40	59.30	56.80	57.10	60.90	57.30	51.10	56.60	60.00	57.10
21.90	22.10	21.20	23.60	21.90	21.80	22.70	21.60	19.20	20.30	20.30	21.80	21.70	19.90	16.50	19.70
1.53	1.50	1.44	2.86	0.87	0.86	2.76	2.05	1.73	0.90	1.94	1.92	1.96	1.87	1.76	1.68
1.79	0.58	0.70	0.55	0.45	0.48	0.23	0.54	0.33	0.24	0.96	0.32	3.13	0.47	0.67	0.33
5.48	4.90	5.84	4.96	5.15	4.95	5.17	4.08	6.46	6.20	3.84	5.39	5.05	5.63	6.47	6.26
8.00	8.73	8.09	7.48	8.95	9.25	8.07	6.85	8.29	8.85	6.40	8.94	7.51	8.62	9.17	8.71
0.008	0.002	0.004	0.013	0.002	0.002	0.024	0.007	0.009	0.003	0.009	0.014	0.010	0.006	0.005	0.005
0.320	0.301	0.215	0.469	0.350	0.356	0.559	0.296	0.272	0.194	0.274	0.344	0.301	0.339	0.202	0.259
0.09	0.08	0.03	0.14	0.08	0.09	0.13	0.06	0.14	0.03	0.06	0.08	0.06	0.22	0.35	0.14
178	71	109	441	69	113	441	315	234	54	268	256	190	212	185	156
22.0	18.0	23.0	22.0	21.0	23.0	22.0	27.0	18.0	21.0	25.0	17.0	20.0	21.0	19.0	23.0
23.0	20.0	28.0	23.0	20.0	21.0	23.0	29.0	16.0	25.0	29.0	19.0	25.0	33.0	25.0	31.0
224.0	204.0	222.0	238.0	202.0	194.0	217.0	226.0	222.0	191.0	205.0	192.0	212.0	225.0	238.0	215.0
144.0	14.0	156.0	234.0	28.0	31.0	112.0	164.0	817.0	232.0	161.0	101.0	166.0	98.0	47.0	32.0
23.0	26.0	27.0	21.0	32.0	31.0	25.0	17.0	9.0	20.0	16.0	22.0	23.0	16.0	14.0	16.0
4.0	5.0	5.0	8.0	4.0	4.0	5.0	9.0	8.0	2.0	7.0	5.0	9.0	6.0	8.0	6.0
250.0	275.0	239.0	277.0	222.0	225.0	343.0	146.0	144.0	187.0	147.0	238.0	148.0	256.0	155.0	200.0
20.0	8.0	13.0	16.0	47.0	20.0	48.0	36.0	36.0	22.0	13.0	29.0	27.0	14.0	43.0	32.0
44.00	17.00	33.00	44.00	31.00	41.00	<15.00	42.0	23.0	19.0	30.0	26.0	13.0	25.0	40.0	21.0
17.0	<15.0	28.0	38.0	38.0	24.0	40.0	31.0	31.0	<15.0	20.0	27.0	15.0	34.0	22.0	29.0
17.0	7.0	19.0	<10.0	12.0	11.0	13.0	8.0	<10.0	<10.0	<10.0	24.0	<10.0	<10.0	8.0	8.0
19.0	18.0	12.0	27.0	12.0	13.0	34.0	24.0	18.0	12.0	32.0	21.0	15.0	16.0	12.0	12.0
14.0	9.0	10.0	17.0	4.0	13.0	20.0	22.0	7.0	13.0	21.0	15.0	20.0	13.0	8.0	7.0
5.0	8.0	7.0	2.0	4.0	5.0	5.0	5.0	2.0	5.0	4.0	5.0	8.0	2.0	9.0	4.0

Kipli 2021      Kipli 2021      Kipli 2021      Kipli 2021      Kipli 2021  
Okopy – 5, Depth 42.0m    Kishinjov – 1, Depth 607.0m    Pidhaytsi – 1, Depth 1252.0m    Sokil – 10, exposure    Pudlivtsi – 92, exposure

56.50	57.30	62.00	56.00	55.90
20.20	17.60	17.60	21.30	21.90
1.75	1.56	1.80	1.42	2.66
0.46	0.75	0.71	0.33	0.36
6.04	6.94	4.84	5.82	4.33

8.56	8.66	7.36	8.29	9.24
0.005	0.005	0.006	0.002	0.004
0.229	0.219	0.262	0.413	0.434
0.25	0.22	0.24	0.09	0.09

157	129	247	60	161
-----	-----	-----	----	-----

24.0	19.0	17.0	21.0	15.0
28.0	26.0	27.0	25.0	24.0
234.0	218.0	222.0	213.0	179.0

90.0	74.0	106.0	22.0	21.0
11.0	14.0	19.0	44.0	42.0
5.0	11.0	6.0	9.0	7.0

149.0	152.0	185.0	288.0	296.0
29.0	39.0	55.0	19.0	24.0
<15.00	54.0	24.0	39.0	15.0
49.0	29.0	30.0	57.0	<15.0

<10.0	<10.0	8.0	9.0	<10.0
11.0	19.0	26.0	13.0	12.0
3.0	7.0	8.0	3.0	18.0
2.0	7.0	4.0	5.0	3.0